~~Was~~ Evidence for Hunga-Tonga eruption influence on the ~~strengthening of the Northern~~ anomalously strong Northern-Hemisphere stratospheric polar vortex in 2024/2025~~associated with the Hunga Tonga eruption?~~

Ales Kuchar[1], Matthias Stocker[2], Alistair Bell[3], Bruno Lehner[1], Jessica Kult-Herdin[1], Gabriel Chiodo[4], Timofei Sukhodolov[5], Eugene Rozanov[5,6], Gunter Stober[3], and Harald E. Rieder[1]

[1]Institute of Meteorology and Climatology, BOKU University, Vienna, Austria
[2]Wegener Center for Climate and Global Change, University of Graz, Graz, Austria
[3]Institute of Applied Physics, Microwave Physics, University of Bern, Switzerland
[4]Instituto de Geociencias (IGEO), CSIC-UCM, Madrid, Spain
[5]Physikalisch-Meteorologisches Observatorium Davos/World Radiation Center (PMOD/WRC), Davos, Switzerland
[6]Ozone Layer and Upper Atmosphere Research Laboratory, Saint Petersburg State University, Russian Federation

Correspondence: A. Kuchar (ales.kuchar@boku.ac.at)

Abstract. The 2022 Hunga Tonga (HT) eruption injected an unprecedented amount of water vapour (WV) into the stratosphere and mesosphere, emerging as a potential multi-year driver of variability in those layers and associated climate feedbacks. Using satellite and reanalysis datasets, and ensemble simulations with the SOCOLv4 model, with and without the HT forcing, we diagnose the chain of processes linking the eruption to the exceptionally strong Northern Hemisphere stratospheric polar vortex (SPV) observed in winter 2024/2025. Satellite data show "tongues" of enhanced WV descending from the mesosphere into the polar stratosphere, collocated with ozone reductions and persistent cold anomalies, alongside a record-strong SPV. Our model with the HT forcing can reproduce the main structure of the descending plume, its effects on chemistry, and the SPV strengthening, albeit with underestimated magnitudes and an earlier onset than observed. Offline radiative transfer calculations indicate that the WV and ozone anomalies drive net radiative cooling over the polar stratosphere, ~~sharpening~~ which steepens meridional temperature gradients and thereby ~~intensifying the~~ intensifies the Arctic polar vortex. The observed 2024/2025 winter thus represents a plausible manifestation of HT-induced vortex variability. Our simulations also predicted the observed shift towards more favorable conditions for sudden stratospheric warmings in the winter 2025/2026 as the WV forcing declines.

1 Introduction

The 2022 Hunga Tonga (HT) eruption was unprecedented in terms of i) injection altitude up to 57 km (Proud et al., 2022), ii) the observational coverage of a direct water vapor (WV) injection of this magnitude (Vömel et al., 2022), and iii) the radiatively-driven plume descent shortly after the eruption due to the highly localized moist volcanic cloud (Kroll and Schmidt, 2024). Many studies have been dedicated to the impacts of the HT eruption, including changes in stratospheric and mesospheric

composition (Evan et al., 2023), radiation (Stocker et al., 2024; Randel et al., 2024b), and direct (Jenkins et al., 2023; Schoeberl et al., 2023; Stenchikov et al., 2025) and indirect (Bednarz et al., 2026; Kuchar et al., 2025) climate impacts.

The WV inputs of HT were distributed throughout the stratosphere, and even to the mesosphere of the Southern Hemisphere subtropics in the days/weeks following the eruption (APARC, 2025). Randel et al. (2024a) documented positive residuals of WV over high latitudes in both hemispheres in late 2023, tied to the downward transport of WV from the HT eruption. Modelling (Fleming et al., 2024; Zhou et al., 2024; Kuchar et al., 2025; Zhuo et al., 2025) and observational (Millán et al., 2022; Schoeberl et al., 2025) studies suggest that the anomalous WV induced by the HT eruption in 2022 should diminish within 5–7 years. The Antarctic dehydration likely remains the dominant WV removal pathway (Zhou et al., 2024), together with transport of stratospheric air to the troposphere at mid-high latitudes by the Brewer-Dobson circulation (BDC). Therefore, we expect that BDC is responsible for the downward transport of WV over middle and high latitudes during the wintertime, in analogy to the downward transport of NO_x, produced by energetic particle precipitation, inside the polar vortex (e.g. Funke et al., 2014).

Kuchar et al. (2025) explored a novel pathway by which water-rich volcanic eruptions, such as HT may modulate stratospheric and mesospheric conditions and influence regional surface climate. Their targeted model simulations illustrated that the excess WV can reduce meridional temperature gradients near the stratopause, leading to a negative Northern Annular Mode anomaly that propagates to the surface in late winter. Several features discussed in Kuchar et al. (2025) were reproduced by an independent atmosphere-only simulation using the NCAR model (Bednarz et al., 2026, and accompanying discussion), including mesospheric cooling at lower latitudes, which, via the thermal wind relation, has the potential to weaken the polar-night jet. Taken together, these studies suggest that HT may have provided favorable conditions for Sudden Stratospheric Warmings (SSWs) observed in NH winters following the HT eruption (Lee et al., 2025).

Various atmospheric (and surface) signals have also been linked to a stratospheric WV increase. Joshi et al. (2006) showed a strengthening of the stratospheric jet in boreal winter associated with the cooler lower stratospheric midlatitudes (increase of meridional temperature gradient) in response to an increased stratospheric WV. Maycock et al. (2013) and Seabrook et al. (2023) reported a similar circulation response. This feature was indeed observed in the winter 2024/2025 when the stratospheric polar vortex was anomalously strong, reaching the climatological maximum ($\sim 61.19\,\mathrm{ms}^{-1}$) on December 24, 2024 (see ~~Fig. 1~~Fig. 1**A** and Section 2.1.1). There were only a few recent winters with a similarly strong and stable polar vortex in the Northern Hemisphere, i.e. 2010/2011, 2015/2016, and 2019/2020 (Manney et al., 2011; Matthias et al., 2016; Lawrence et al., 2020; Rieder et al., 2025).

Motivated by the diverse findings of HT impacts summarized in the recent dedicated report (APARC, 2025), our study seeks to extend the portfolio of pathways by which the HT eruption may have modulated stratospheric and mesospheric conditions and consequently impacted the surface climate. Specifically, we aim here to answer the following questions: i) How does the long-term response of the stratospheric polar vortex (SPV) to atmospheric composition changes following the HT eruption differ from the short-term response? ii) Did atmospheric composition changes precondition SPV states, particularly the strong SPV observed in 2024/2025? and iii) if so, which predictive power can be derived from comprehensive chemistry-climate model simulations for SPV states in the coming years?

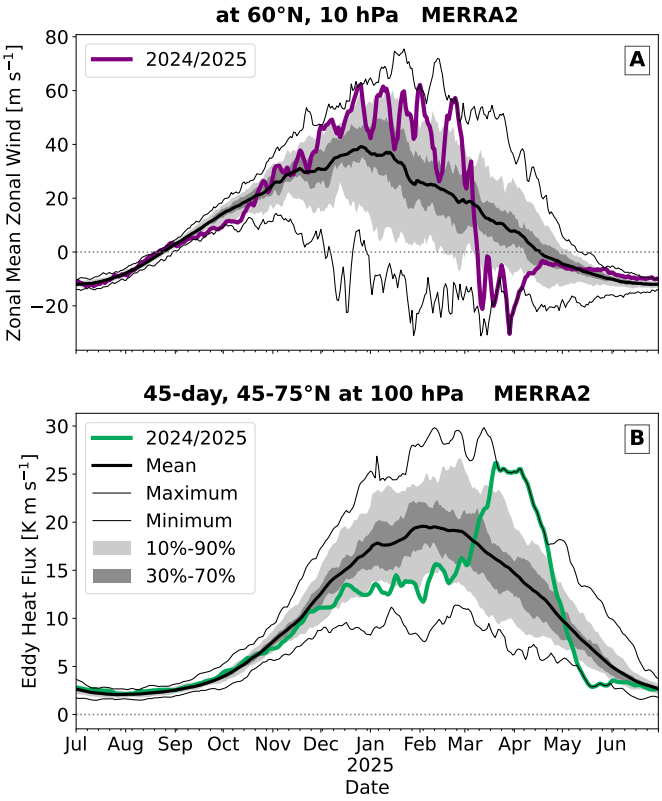


Figure 1. A: The average (east-west) zonal wind for 60°N at 10 hPa for the extended winter 2024/2025 (OW3) in MERRA2. This is near the peak of the polar jet maximum. **B**: The eddy heat flux (EHF) averaged between 45°N and 75°N at 100 hPa for the 45 days before the date indicated.

To this end, we provide a combined observational and modelling assessment of the 2024/2025 event and its linkages to the lingering Hunga-induced moist plume. We use a reanalysis and observations from MLS and SWOOSH (Section 2.1), together with large-ensemble SOCOLv4 simulations with and without the HT forcing (Section 2.2), to investigate the sensitivity of the circulation to excess WV from HT and assess the chain of processes leading to SPV strengthening (Section 4).

2 Data

2.1 Observational datasets

2.1.1 MERRA2

Here we analyze a widely used reanalysis data set, the National Aeronautics and Space Administration (NASA) Modern Era Retrospective Analysis for Research and Applications Version 2 (MERRA2, resolution $0.625° \times 0.5°$, model top at 0.01 hPa; Gelaro et al.,

. We extract zonal wind (ZW) for 60°N at 10 hPa and eddy heat flux (EHF) between 45°N and 75°N at 100 hPa postprocessed by the NASA Ozone Watch (Kramarova and Lait, 2025) for the extended winter 2024/2025.

2.1.2 MLS

The Microwave Limb Sounder (MLS; Waters et al., 2006) instrument onboard NASA's Aura Satellite has been operational since 2004 and provides near-global (82°S—82°N) measurements of key atmospheric constituents and temperature based on thermal microwave emissions along the Earth's limb. The MLS provides about 3500 vertical profiles per day for each species. The profiles have a vertical resolution of approximately 3 to 5 km in the stratosphere and 6 to 8 km in the mesosphere. In this study, we use Version 6 of the retrieval products for water vapor, ozone, and temperature (Livesey et al., 2026).

Since May 2024, the 190 GHz subsystem in MLS, which is responsible for observing water vapor, N_2O, HCN, and upper stratospheric HNO_3, has been operating on a duty cycle to extend the instrument's lifetime (see https://mls.jpl.nasa.gov/). The measurements are reactivated for about six days in the middle of each calendar month. Other MLS channels, including those used for ozone and temperature, remain unaffected.

Water vapor, temperature and ozone data were processed using the recommended MLS quality screening (QS) criteria.

2.1.3 SWOOSH

The Stratospheric Water and Ozone Satellite Homogenized (SWOOSH) version 2.72 dataset provides zonally averaged monthly profiles for water vapor and ozone. SWOOSH combines measurements from several satellite sensors, including the Stratospheric Aerosol and Gas Experiment (SAGE II & III), the Upper Atmosphere Research Satellite Halogen Occultation Experiment (UARS HALOE), UARS MLS, and Aura MLS version 5.0. The retrieval artifact in the 10—8 hPa layer apparent in SWOOSH (see Fig. 2 and Niemeier et al. (2023); Millán et al. (2024)) has been corrected in the MLS data version 6 we use in this study. To account for measurement offsets and biases, the data records were homogenized using „reference" satellites during times in which observations of different satellite systems overlapped. The satellite that showed the best agreement with balloon-based measurements was chosen as a reference (Davis et al., 2016b).

2.2 SOCOLv4 simulations

Our set of SOCOLv4 (Sukhodolov et al., 2021) simulations comprises an ensemble of transient simulations with and without the HT forcing, with 5-year spin-up before the HT eruption. Both ensembles comprise 10 ensemble members. We stress that the Quasi-Biennial Oscillation (QBO) is nudged in both simulations with and without the HT forcing. We can demonstrate a link between the equatorial ZW at 10 hPa (QBO phase) and the polar vortex in SOCOLv4, i.e. so called Holton-Tan mechanism (Holton and Tan, 1980). For a detailed description of our SOCOLv4 simulations, we refer to Section A1 in Kuchar et al. (2025) .

As indicated in Kuchar et al. (2025), the anomalous WV following HT dissipates in SOCOLv4 quicker than observed (cf. globally averaged WV anomaly in SOCOLv4, MLSv6 and SWOOSH in Fig. 2) or some of the other models (Randel et al., 2024b)

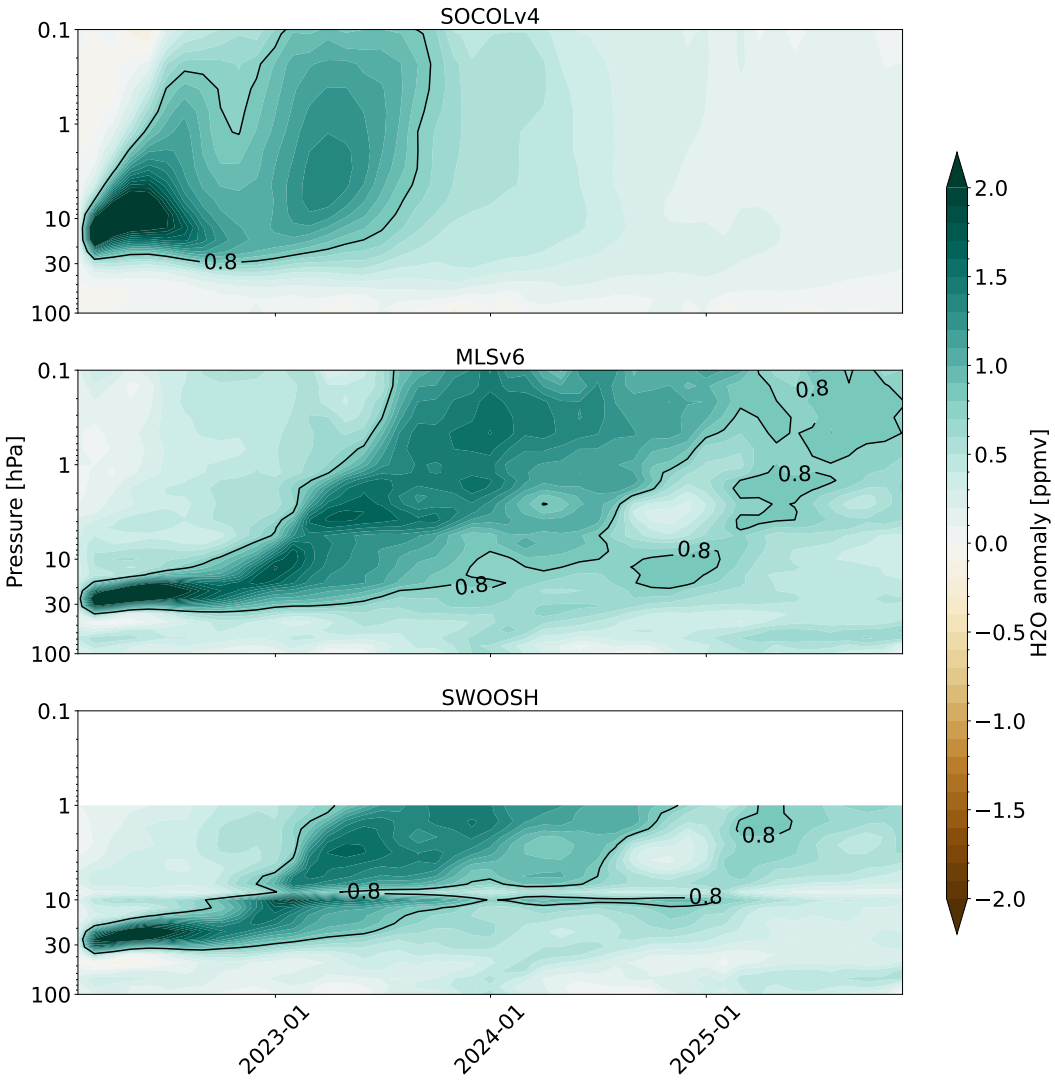


Figure 2. Globally averaged water vapour (WV) anomalies (shading and contours for 0.8 ppmv) in SOCOLv4, MLSv6 and SWOOSH for the period 202201–202511. The 10–8 hPa artifact (Millán et al., 2024) in WV is still apparent in SWOOSH since it contains data from MLSv5.0 (Davis et al., 2016a).

. Note that the contour for 0.5 ppmv does not reach the year 2024 in SOCOLv4 as in SWOOSH. It is questionable whether this bias is due to a different initialization (Zhu et al., 2025) or a model bias related to overly fast transport already reported in Sukhodolov et al. (2021) or Arsenovic et al. (2019). This longstanding issue persists even in the newest generation of chemistry-climate models, and SOCOLv4 is consistent with other models across generations (Abalos et al., 2026). Overall, SOCOLv4 is adequate for broad NOx/HOx/ClOx driven ozone depletion/recovery studies (Sukhodolov et al., 2021). The main remaining weaknesses are transport and mixing, and photolysis at large solar zenith angles over the high latitudes of the Southern Hemisphere (e.g. Imanova et al., 2

.

3 Methods

3.1 Offline radiative transfer simulations

We prescribed WV and ozone anomalies from MLS for the extended winter 2024/2025 (OW3) and calculated longwave and shortwave radiative heating rates using *konrad* (Kluft et al., 2019; Dacie et al., 2019). *Konrad* uses interfaces to the Rapid Radiative Transfer (RT) Model for GCMs (RRTMG; Kroll et al., 2021). We state that these radiative calculations are robust for various solar zenith angles.

3.2 Calculation of anomalies

Throughout our analysis, we evaluate significance fields using the minimum local p-values from Student's t-test with global test statistics. Most of the illustrations in Section 4 show differences between simulations with and without the HT forcing.

3.3 Eliassen-Palm flux diagnostics

We investigate the response of resolved planetary waves (PWs) using the Eliassen-Palm flux diagnostics (EPF; Andrews and McIntyre, 1987

. EP fluxes are computed and scaled following Jucker (2021). The EPF convergence serves as an indicator of wave dissipation, and the EPF divergence (EPFD) indicates sourcing. We illustrate all EPF diagnostics from 2023-10-01 to 2024-03-30 in supplementary figure `EPFD_plot_2023-2024.pdf`.

3.4 Calculation of Southern Oscillation Index (SOI)

We calculate the Southern Oscillation Index (SOI) using sea level pressure (SLP) standardised difference between Tahiti (17.65°S, 149.45°W) and Darwin (12.46°S, 130.84°E) as a proxy for the El Niño Southern Oscillation (ENSO). Negative and positive SOI values coincide with abnormally warm and cold ocean waters across the eastern tropical Pacific typical of El Niño and La Niña episodes, respectively.

4 Results

4.1 Observed changes in water vapor, ozone, and temperature

We set the scene by illustrating the daily evolution of stratospheric dynamics in the extended winter 2024/2025 (the third observed winter after the HT eruption; thus, marked as OW3) using the MERRA2 reanalysis in ~~Fig. 1.~~ Fig. 1. Here, the zonal-mean winds diagnosed at 60°N at 10 hPa illustrate that the SPV strength exceeds the average strength ~~in~~ during DJF 2024/2025. Next, we turn the focus to anomalies of WV, temperature, and ozone (derived from the MLS observations in ~~Fig. 3~~Fig. 3), to put the exceptionally strong SPV in the context of the lingering HT perturbation in polar latitudes. The WV anomalies (see ~~Fig. 3~~Fig. 3**A**) are characterized by "tongues" with concentrations of up to 2 ppmv. The first tongue appears in the mesosphere during ~~October/November~~ September 2024 and continuously propagates downward with time to ∼10 hPa, where it gradually weakens and dissipates by March 2025, when it merges with the stratospheric background. A second tongue forms in the mesosphere in January 2025 and also propagates downward (not shown for the chosen time frame of Fig. 3). The WV anomaly is statistically significant[1] over much of the descending tongue. In contrast, the negative ozone and temperature anomalies are statistically significant only locally, mainly along the upper flank of the WV tongue starting around 0.1 hPa in September and ending below 10 hPa in February (see ~~Fig. 3~~Fig. 3**B, C**), reflecting the large daily and interannual variability of polar ~~winter~~ wintertime conditions. We therefore do not interpret the 2024/2025 anomalies as uniquely attributable to HT; rather, the observations indicate a plausible HT contribution superimposed on internal dynamical variability. The temperature anomalies are followed by their positive counterparts. By October, an enhanced ozone anomaly (~ 0.5 ppmv) emerged around 10 hPa, leading to effective warming due to ozone absorption of solar radiation and increased mixing ~~(see Fig. 8)~~ and thereby masking the WV-induced cooling propagating downward. In March, we observe a significant increase and decrease in stratospheric and mesospheric polar temperatures, respectively. However, the stratospheric ozone anomalies have both ~~both~~ alternating positive and negative bands. This corresponds to the stratospheric final warming during which the SPV does not recover and transitions to summer conditions, with easterly winds across the stratosphere (see ~~Fig. 1~~Fig. 1**A**). The observed stratospheric and lower-mesospheric longwave cooling rates are dominated by CO_2 together with ozone and WV (Clough and Iacono, 1995; Brasseur and Solomon, 2005). The close correspondence between the WV and ozone anomalies and the diagnosed temperature response suggests the radiative cooling observed in OW3. However, ~~comparing~~ a comparison with OW2 (see Fig. 4) implies that slowly descending WV, i.e. dynamical preconditioning (see ~~eddy heat flux (EHF)~~ EHF in Fig. 1**B**)~~positively feedbacks~~, positively feeds back on radiative cooling and strengthens the vortex. We examine this mechanism explicitly in the model simulations below.

4.2 Modeled changes in water vapor, ozone, and temperature

The downward propagating tongue of WV during winter is captured in our SOCOLv4 ensemble. The feature emerges in the extended winter 2023/2024 (marked as the second model winter after the HT eruption, MW2; see ~~Fig. 5~~Fig. 5**A**) and winter of

[1] at respective p-values for given figure

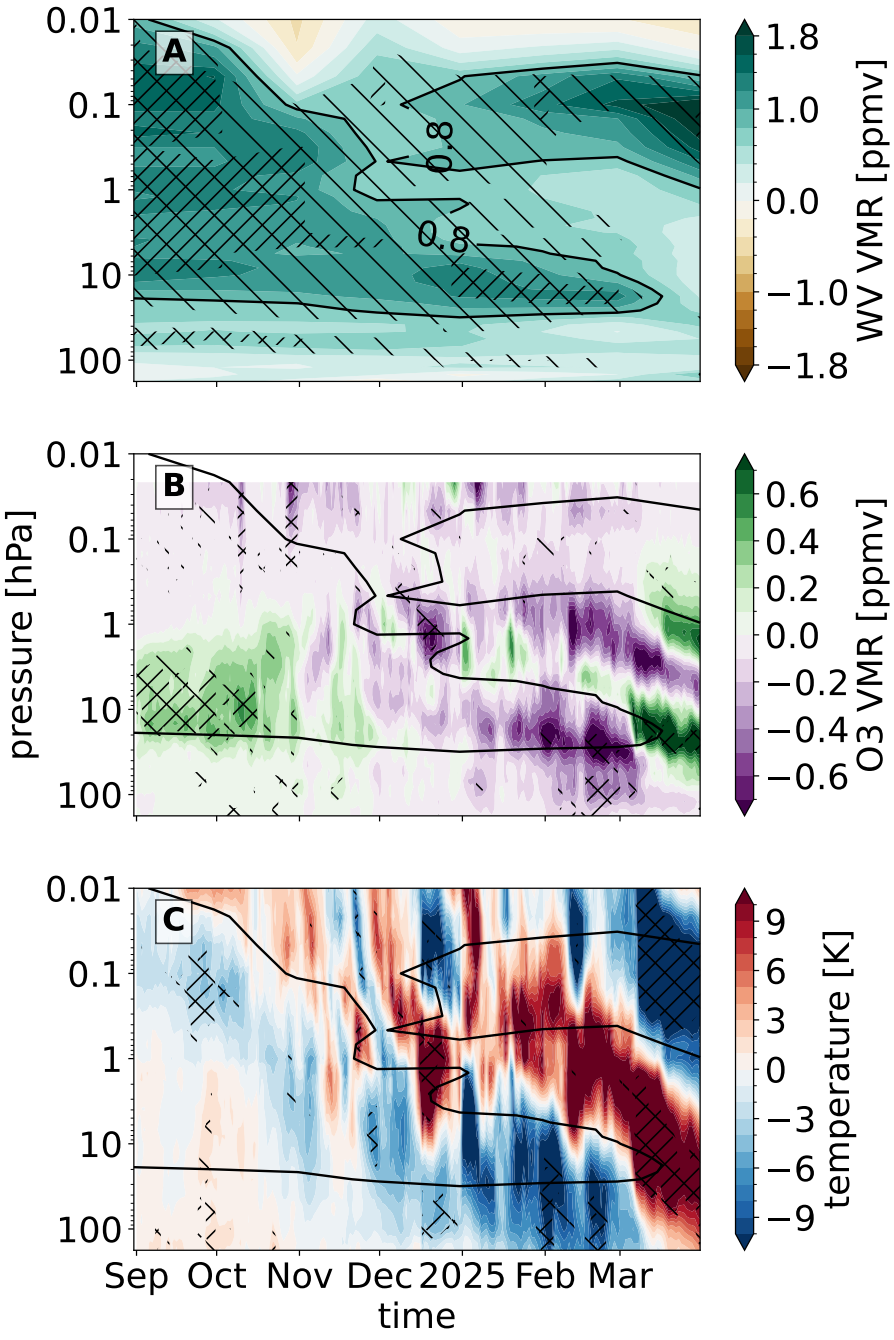


Figure 3. Zonal mean weighted average for latitudes between 60°–90°N of water vapour volume mixing ratio (VMR; shading in **A** and contour of 0.8 ppmv in **B** and **C**; in ppmv; monthly), ozone VMR (shading in **B**, in ppmv; daily) and temperature (shading in **C**; in K; daily) and anomalies for the extended winter 2024/2025 (OW3) from MLS. Anomalies are expressed as differences with respect to the climatology for the period 2006–2020. Hatching \\\\ and //// show where the empirical two-sided p-values are < 0.1 and < 0.05, respectively. Due to missing data, water vapour is visualized as monthly anomalies with interpolated gaps.

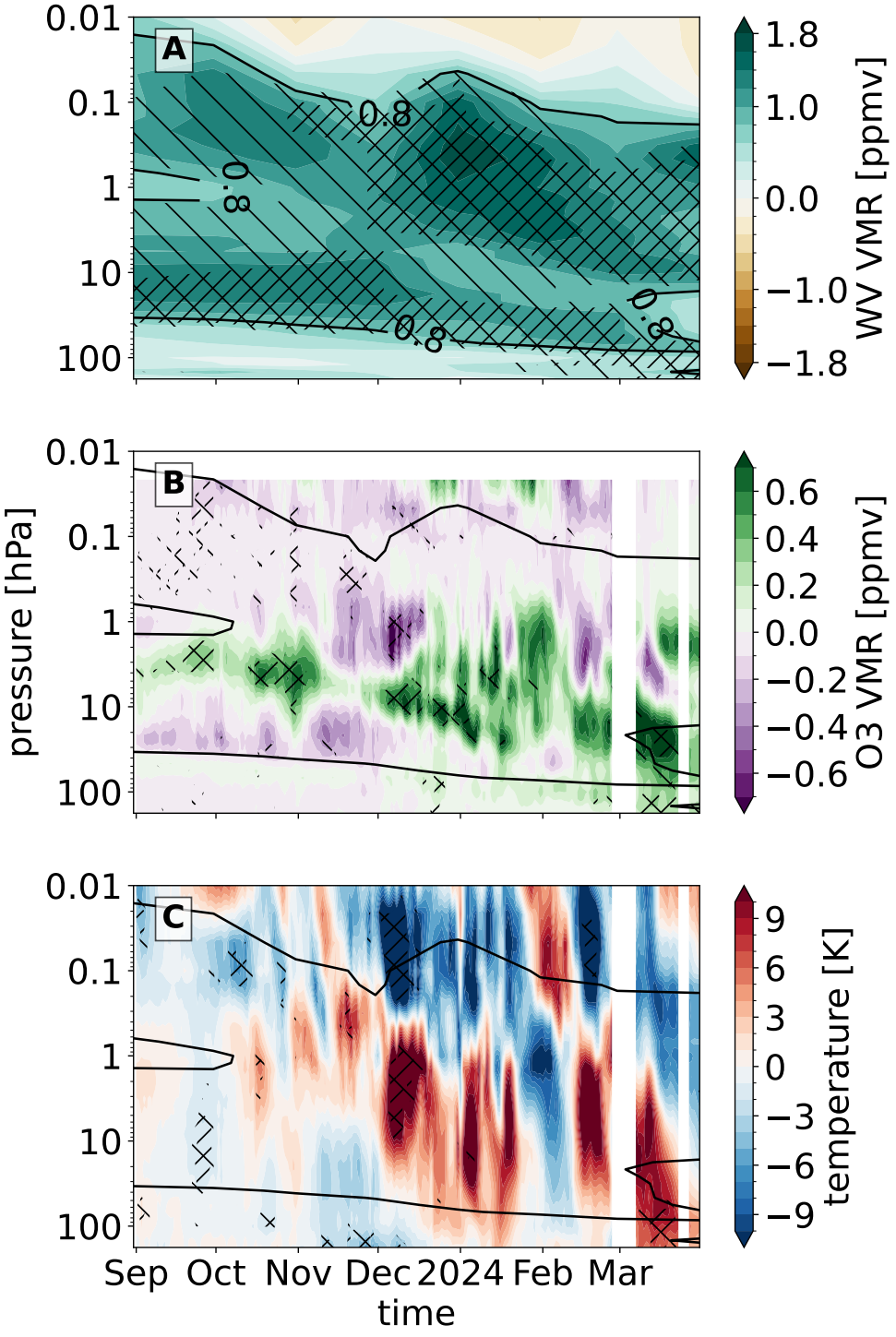


Figure 4. As Fig. 3 but for the extended winter 2023/2024 (OW2).

2024/2025 (MW3; see Fig. 6**A**). The WV enhancement is, however, underestimated compared to observations in ~~Fig. 3~~Fig. 3 **A**, especially in MW3. Given the ~~well documented~~ well-documented model deficiency of accelerated transport of SOCOLv4 (discussed in detail in Section 2.2), we argue that the winter MW2 in our simulations corresponds to OW3 in observations (see Section 4.1 and Fig. 3). For the MW2 SOCOLv4 yields a similar strengthening of the vortex with ~~not as pronounced weakening as~~ a less pronounced weakening than observed at the end of OW3 (cf. Fig. 5**D** at 10 hPa and Fig. 1**A**). In analogy, we assume MW3 matches with the upcoming OW4, as we detail further below.

For MW2 (equaling OW3) we attribute the initial ozone destruction in the upper stratosphere and lower mesosphere to increased OH concentrations induced by the excess WV from the HT eruption (HO_x cycle) and the ClO_x activation from chlorine reservoirs (see Fig. 7). These coincide with a negative anomaly in NO_x mainly attributable to cooling at these levels (Fleming et al., 2024). In contrast, as reported in Fleming et al. (2024); Kuchar et al. (2025), the positive ozone anomaly limited ~~in~~ to Sep-Nov and rather in the lower to mid stratosphere, similar to MLS, emerges due to increased conversion of NO_x to the HNO_3 reservoir given an overall higher abundance of OH. While negative ozone and negative temperature anomalies are not statistically significant[1] along the entire WV tongue similarly as in observations (see Fig. 3), they are associated with a stronger SPV and correspondingly weaker poleward transport of ozone from lower latitudes reflected by the EHF (see red line Fig. 5**D** and Fig. 8). Thus, the paired SOCOLv4 ~~ensemble indicates a forced tendency toward stronger westerlies under HT forcing, not deterministic attribution of~~ simulations indicate that HT forcing shifts the ensemble-mean circulation response toward stronger polar westerlies. However, this ensemble-mean response does not imply that individual ozone, temperature, or wind anomalies, or the full observed evolution of OW3, can be uniquely attributed to the HT forcing.

Next, we investigate the radiative effect of the observed changes in WV and O_3 on temperature via offline radiative transfer (RT) calculations (see Section 3.1). These RT calculations presented in Fig. 9 reveal that perturbations in both WV and ozone abundances are capable of inducing cooling rates in the order of -0.5 to ~~$-1\,\mathrm{K/day}$~~ $-1\,\mathrm{K\cdot day^{-1}}$, with WV and ozone dominating the change in the longwave and shortwave heating rates throughout the stratosphere and in the upper layers, respectively. These heating ~~rates~~ rate anomalies are collocated with those observed (see Fig. 3**C**) and simulated (see Fig. 5**C**). SOCOLv4, however, does yield a weaker temperature response initially, attributable to weaker changes in shortwave heating rates following the weaker ozone anomaly than seen in the MLS observations.

We confirm these calculations using precise line-by-line RT simulations (Bell et al., 2025). The resulting longwave heating rates from prescribed time-evolving WV and ozone from SOCOLv4 are shown in Fig. 10.

As detailed in Bloxam and Huang (2021), the radiative-cooling recovery of SSW-induced temperature anomalies in the absence of dynamical heating is dominated by longwave radiative cooling, and is characterized by increasing e-folding times from the upper to middle stratosphere. If we invert the e-folding times ($4-7.5$ days in the upper stratosphere) of Bloxam and Huang (2021), we obtain an equivalent heating-rate effect of roughly $0.13-0.25\,\mathrm{K\cdot day^{-1}}$ per K. Given that the e-folding time increases in the lower stratosphere and decreases in the mesosphere, we expect that temperature perturbations translate into weaker and stronger heating-rate effects at lower and upper levels, respectively. In the lower stratosphere, the air cools more slowly because there is a deeper layer of atmosphere above it that absorbs the radiation, re-emits it upwards but also downwards, and

[1] ~~at respective p-values for given figure~~

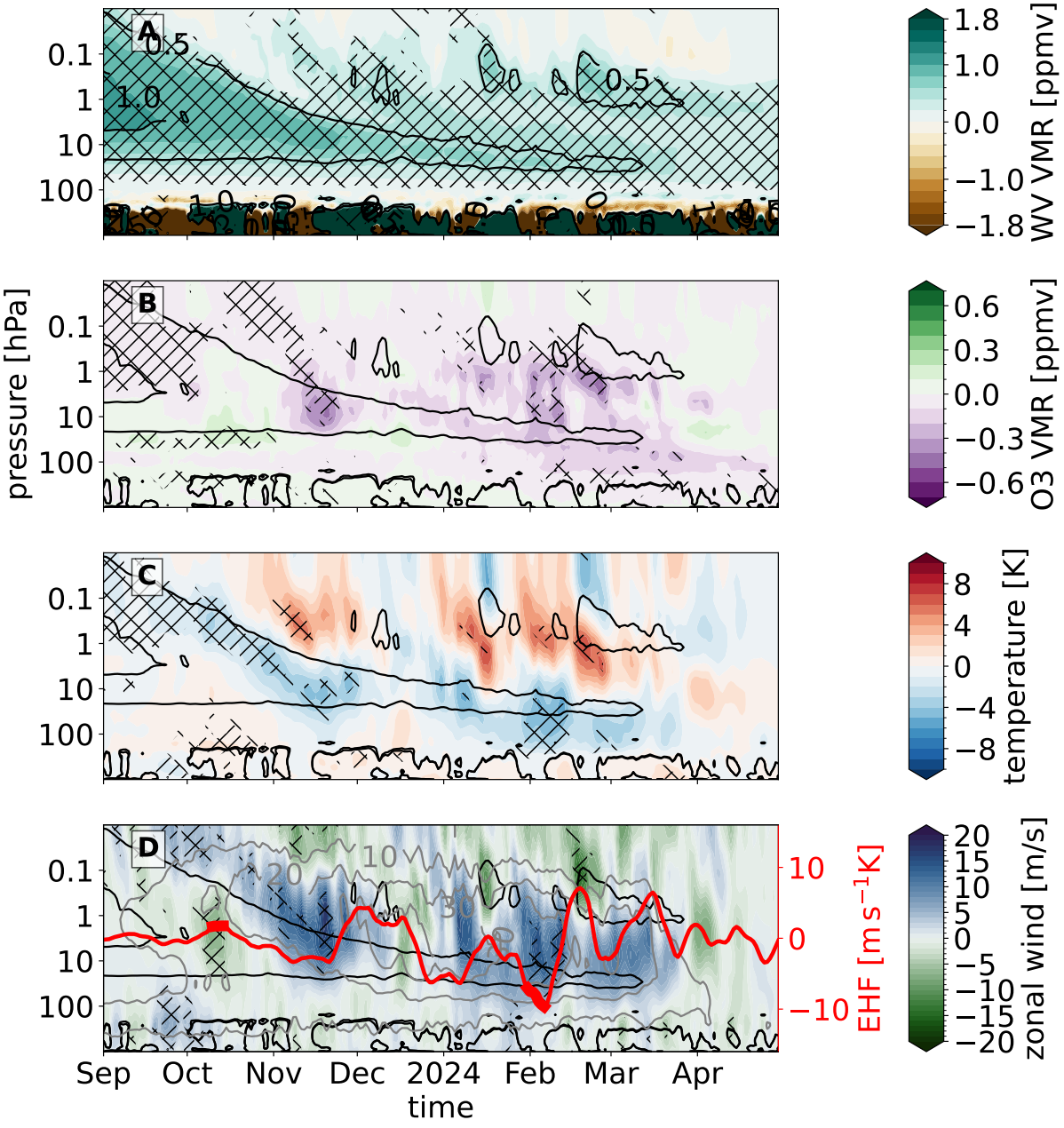


Figure 5. Weighted zonally-average over 60°–90°N of water vapour volume mixing ratio (VMR; shading in **A** and contours of 0.5 and 1 ppmv in **A**, **B**, **C** and **D**; in ppmv), ozone VMR (shading in **B**, in ppmv), temperature (shading in **C**; in K), and zonal wind at 60°N (shading in **D**) and Eddy Heat Flux at 100 hPa averaged over 45°–75°N (EHF in $\mathrm{m/s\,K}$; red line in **C**) daily anomalies for the extended winter 2023/2024 (MW2) from SOCOLv4. Anomalies are expressed as the difference between the SOCOLv4 simulation with and without the HT forcing. Hatching \\\\ and //// show where the p-values of the t-test are < 0.1 and < 0.05, respectively. Gray contours in **D** represent absolute values of zonal wind in the SOCOLv4 simulation with the HT forcing.

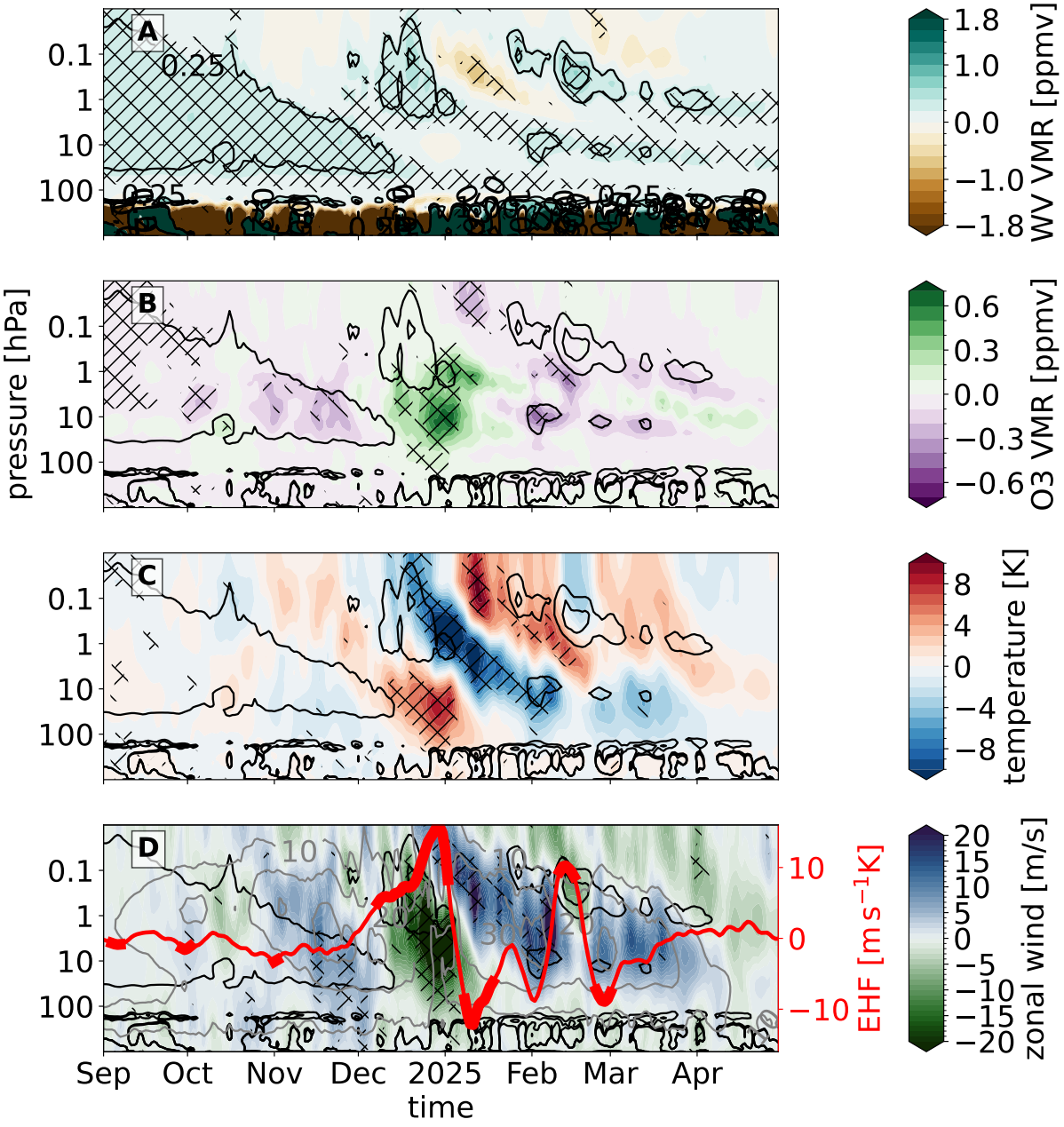


Figure 6. As in Fig. 5 but for the extended winter 2024/2025 (MW3).

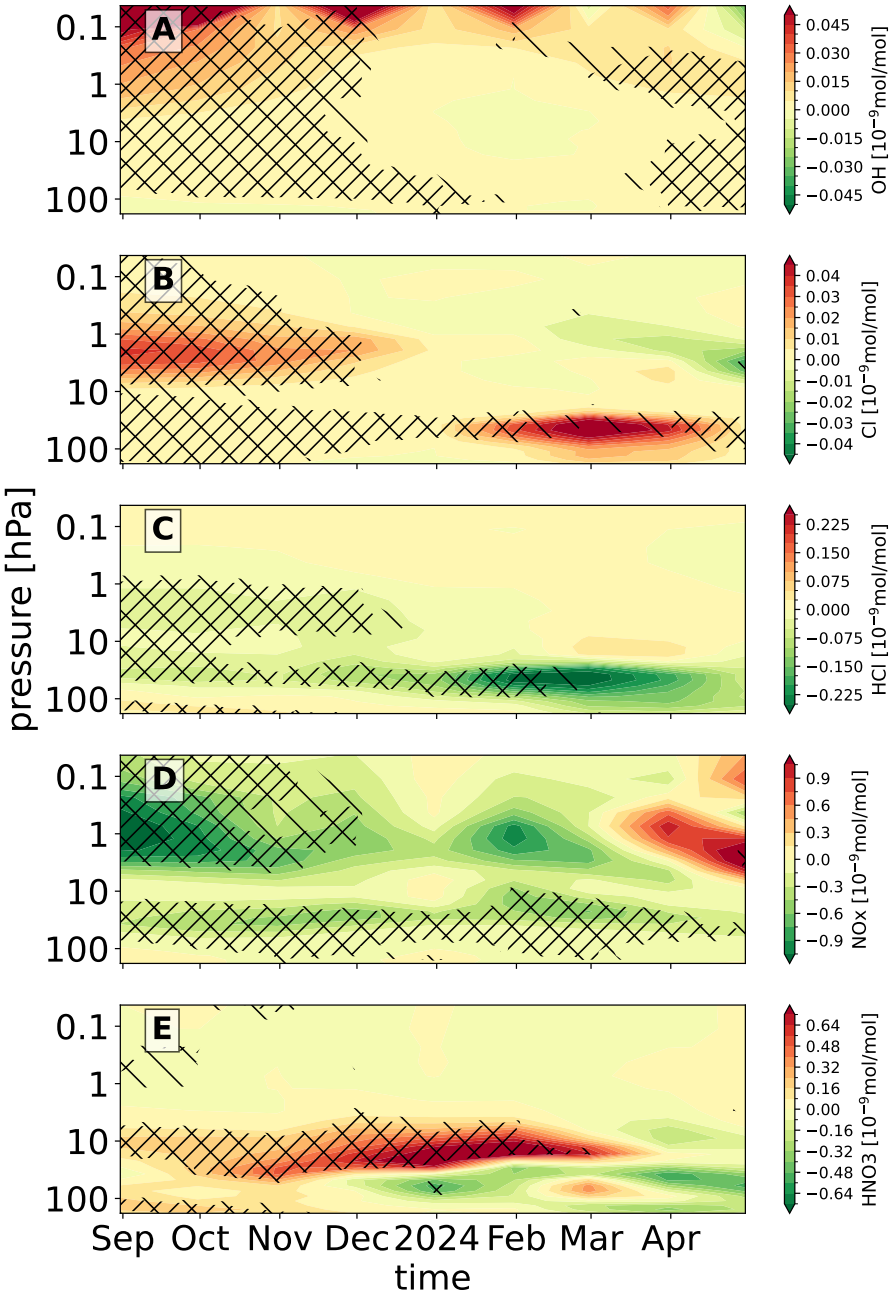


Figure 7. Monthly zonal-mean anomalies of polar chemistry for the period 2023/2024 (MW2). Anomalies are expressed as the difference between the SOCOLv4 simulation with and without the HT forcing. Hatching \\\\ and //// show where the p-values of the t-test are < 0.1 and < 0.05, respectively.

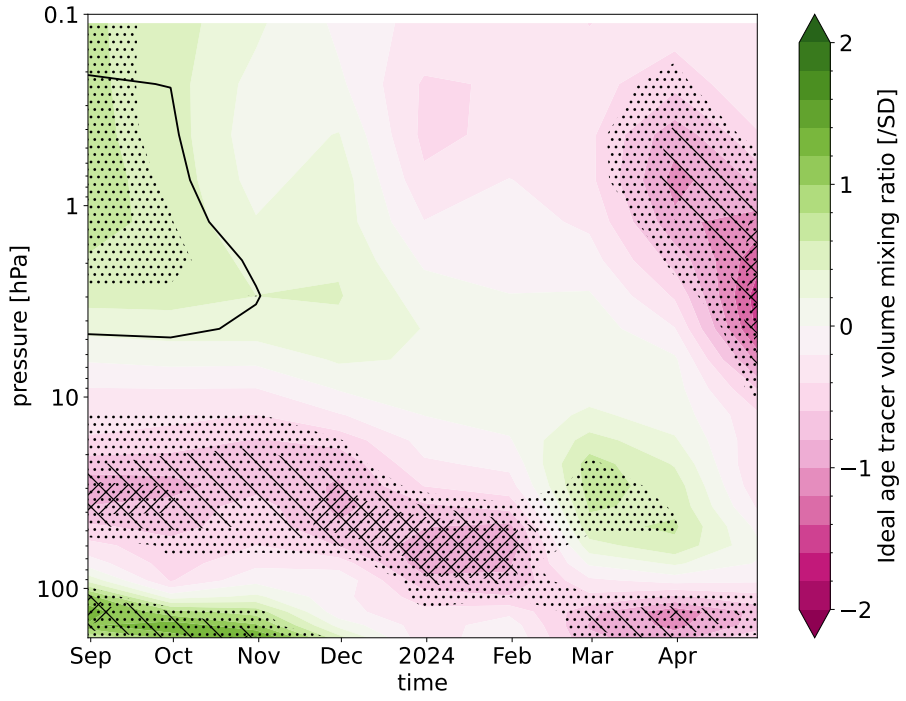


Figure 8. Weighthed zonally-average over 60°–90°N of age of air estimated as idealized age tracer volume mixing ratio monthly anomalies for the extended winter 2023/2024 (MW2). Anomalies are expressed as the difference between the SOCOLv4 simulation with and without the HT forcing and normalized to its climatological standard deviation (SD). Dots ... and hatching \\\\ and //// show where the p-values of the t-test are < 0.3 and < 0.1 and < 0.05, respectively. The black contour line represents the contour of 1 ppmv of water vapour anomaly.

thereby effectively reduces the amount of energy that can escape into space. Closer to the tropopause, the cooling effect reduces as the radiation emitted depends strongly on the background temperature itself (Bloxam and Huang, 2021). This asymmetry may explain the different persistence of the heating rate anomalies at different heights that appear in Fig. 10**B**. Furthermore, the pronounced positive heating rate anomaly around 1 hPa spanning from December 2024 to March 2025, consistent with enhanced longwave heating related to decreased ozone, aids in explaining the rapid change from negative to positive temperature anomalies (see Fig. 3**B** and Fig. 5**C**).

The negative temperature anomalies throughout the upper stratosphere and lower mesosphere result in an enhanced meridional temperature gradient (see Fig. 14), which strengthens ~~,~~ SPV via the thermal wind balance~~, SPV~~. The SPV strengthening may initially enhance vertical wave propagation during October, a time when ~~zonal winds (ZW)~~ ZW are usually weak and thus allow more ~~planetary waves (PWs)~~ PWs to propagate upwards into the stratosphere (Charney and Drazin, 1961). In this respect, we understand the simultaneously observed anomalously high EHF at 100 hPa (see ~~Fig. 1~~Fig. 1**B**) as a proxy for upward propagation of PWs (e.g. Newman et al., 2001). This way we associate the anomalously weak ZW below in the stratosphere ~~due~~ to anomalously breaking PWs (see visualization of EPF in supplementary figure, Section 3.3). As the cooling progresses

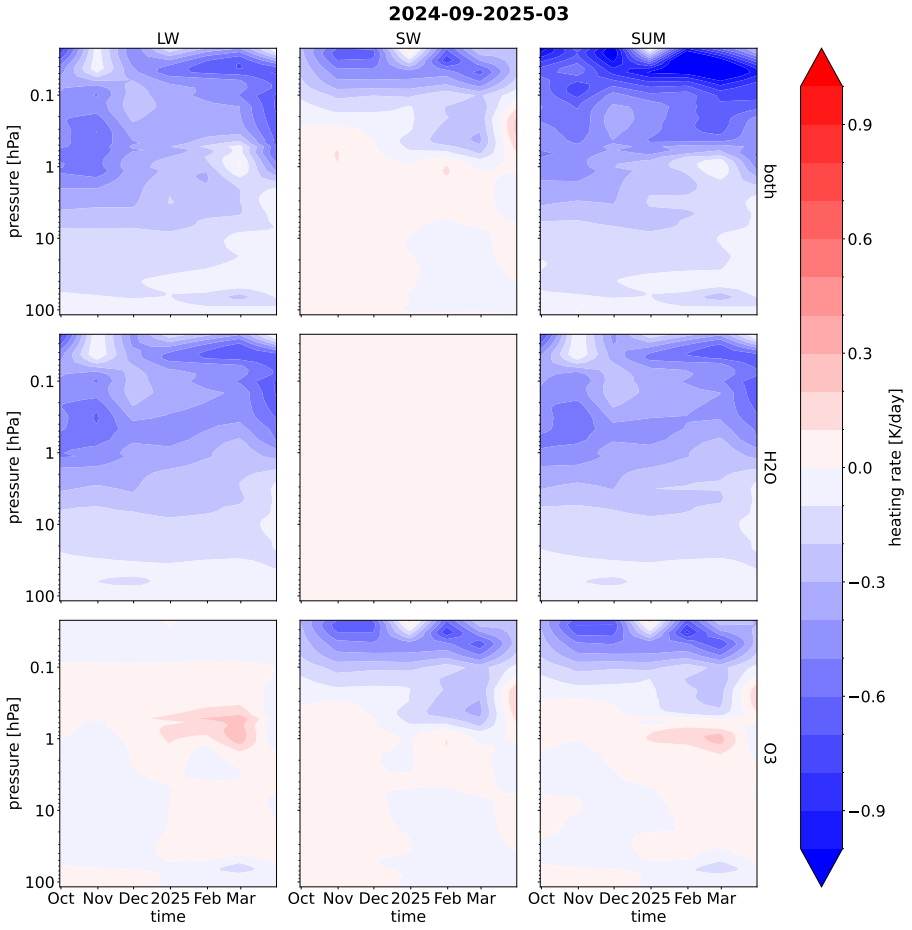


Figure 9. RRTMG radiative heating rates (longwave, shortwave and their sum) for prescribed weighted zonally-average over 60°–90°N of water vapour and ozone monthly anomalies from MLS for the extended winter 2024/2025 (OW3).

downward, it aids the strengthening of the winds, which tend to be too strong for wave propagation (Plumb, 1989). This may confirm the nonlinearity of SPV for generally large wave forcing during the NH winter conditions (Scott and Haynes, 2002). The stronger SPV is associated with pronounced negative and positive temperature anomalies below and above, respectively. A similar dipole structure has been discussed in studies diagnosing SH high-latitude temperature trends as a consequence of ozone depletion (e.g Young et al., 2013; Keeble et al., 2014). Manzini et al. (2003) attributed the positive temperature anomaly at upper levels to increased downwelling, and thus, consequently, adiabatic warming due to enhanced gravity wave propagation. Correspondingly, stronger westerlies in the stratosphere filter eastward gravity waves while westward gravity waves propagate freely upward and deposit their momentum above.

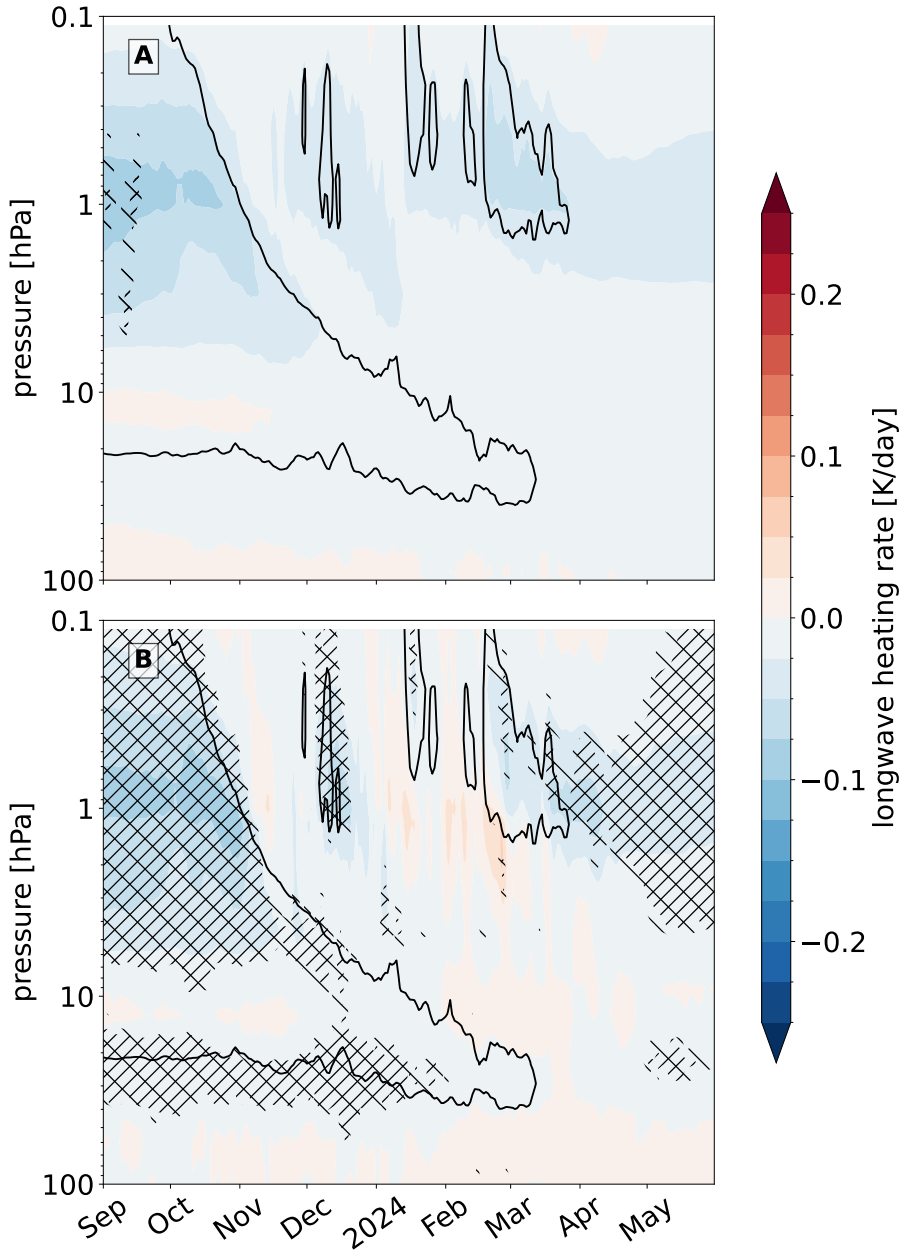


Figure 10. Weighted zonally-average over 60°–90°N of clear-sky (offline) longwave heating rate (in $K \cdot day^{-1}$) anomalies calculated using solely WV (shading in **A**); WV and O_3 (shading in **B**). Contour in all panels represents a WV anomaly (0.5 ppmv) as in Figure 5. Anomalies are expressed as the difference between the SOCOLv4 simulation with and without the HT forcing. Hatching \\\\ and //// show where the p-values of the t-test are < 0.1 and < 0.05, respectively.

4.2.1 QBO and ENSO preconditioning

As for MW2, we find similar "tongues" of WV and downward propagation of ozone in the SOCOLv4 simulations for MW3 (see Fig. 6). Here, however, the excess of WV only yields up to 0.25 ppmv, and thus a much smaller magnitude compared to ~~MW2 and~~ OW3 by MLS. This reduced WV forcing results only in a subtle cooling, which slightly strengthens the ZW, before they significantly weaken as a consequence of anomalously high EHF in December 2024 and the beginning of January 2025. This episode is followed by a recovery of SPV and collocated negative temperature anomaly propagating from the lower mesosphere to the lower stratosphere~~(discussed in detail in Section 4.2.1). In Section 4.2.1 we also argue that the~~ .

The episode with the weakened ZW as a consequence of anomalously high EHF in December 2024 (MW3 in Fig. 6) and the beginning of January 2025 can be traced back to two main clusters of ensemble members in the simulations with the HT forcing (see Fig. 11). While one major cluster of 4 ensemble members (with mixed Southern Oscillation Index (SOI) preconditioning) strengthens SPV, the other cluster of 6 ensemble members (with mostly positive SOI (see Fig. 12) corresponding to La Niña preconditioning) weakens the stratospheric winds leading to the emergence of SSWs between December 2024 and January 2025. Considering the easterly phase of QBO at 10 hPa for MW3, we hypothesize that this may have preconditioned the latter cluster to a higher probability of weaker SPV or SSWs, respectively. Such interpretation is consistent with the observation that SSWs are more likely to occur during easterly QBO in tandem with either El Niño or La Niña conditions (Lee et al., 2025).

That said, the simulated equatorial winds in the westerly QBO phase during the early stage of MW2 (see Fig. 12) create conditions that favor a stronger SPV, consistent with the Holton–Tan mechanism (Holton and Tan, 1980). A similar configuration occurred in OW3, when the QBO was also in its westerly phase[2]. Since the QBO preconditioning is identical in both simulations (with and without the HT forcing) and ENSO is uniformly sampled in SOCOLv4, encompassing both El Niño (SOI<0) and La Niña (SOI>0; as ultimately observed in OW3), we infer that the forced SPV response in MW2 arises from the HT-induced WV compared to OW3 where perhaps both QBO and the HT forcing contributed to the stronger SPV.

From the SOCOLv4 ensemble, yielding one cluster with easterly QBO and La Nina conditions in MW3, we hypothesize that the winter 2025/2026 (OW4) bears an enhanced probability ~~for SSW occurrence, which actually happened in March in reality~~of SSW occurrence. As the associated wind pattern propagates downward, we consequently identify a SLP pattern characteristic of a weaker SPV, i.e., a positive SLP anomaly at the poles and a negative SLP anomaly at the mid-latitudes (see Fig. 13).

~~Weighted zonally-average over 60°–90°N of water vapour volume mixing ratio (VMR; shading in **A** and contours of 0.5 and 1 ppmv in **A**, **B**, **C** and **D**; in ppmv), ozone VMR (shading in **B**, in ppmv), temperature (shading in **C**; in K), and zonal wind at 60°N (shading in **D**) and Eddy Heat Flux at 100 hPa averaged over 45°–75°N (EHF in $\mathrm{m/s K}$; red line in **C**) daily anomalies for the extended winter 2023/2024 (MW2) from SOCOLv4. Anomalies are expressed as the difference between the SOCOLv4 simulation with and without the HT forcing. Hatching \\\\ and //// show where the p-values of the t-test are < 0.1 and < 0.05, respectively. Gray contours in **D** represent absolute values of zonal wind in the SOCOLv4 simulation with the HT forcing.~~

~~As in Fig. 5 but for the extended winter 2024/2025 (MW3).~~

[2]https://www.climate.gov/news-features/blogs/polar-vortex/predicting-chances-polar-vortex-disruption-winter

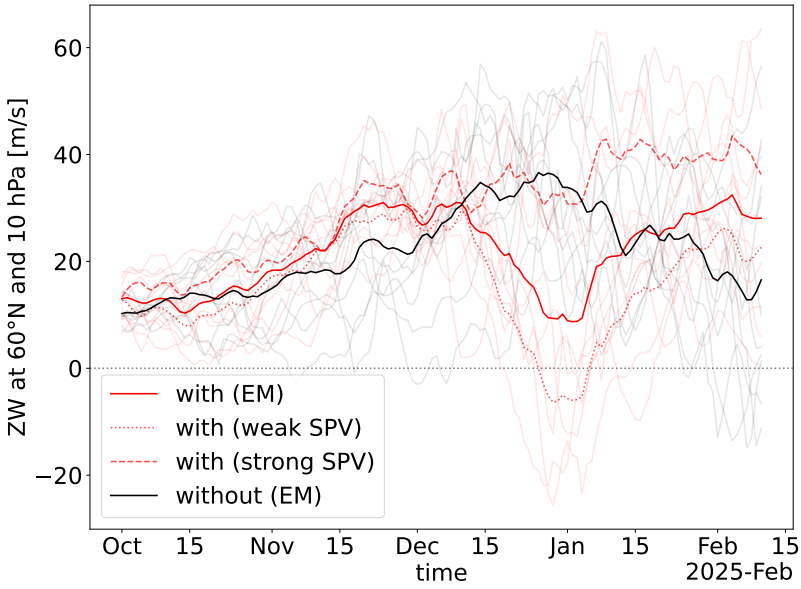


Figure 11. Daily zonal-mean zonal wind at 10 hPa and 60°N based on the SOCOLv4 simulation with (ensemble mean (EM); red solid line) and without (black solid line) the HT forcing for the period 2024/2025 (MW3). The SOCOLv4 simulation with the HT forcing reveals two clusters: weak SPV (red dotted line) and strong SPV (red dashed line).

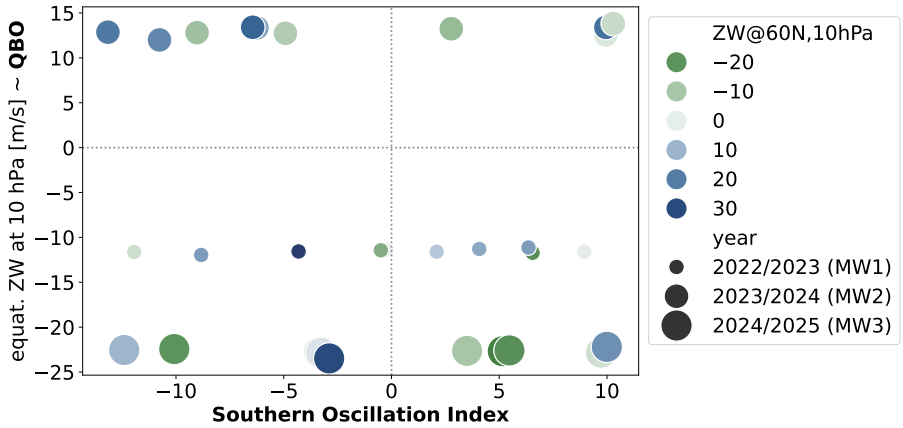


Figure 12. Scatter plot of equatorial zonal wind at 10 hPa as a proxy for Quasi-biennial Oscillation (QBO) in SOCOLv4 and Southern Oscillation Index (SOI) in the simulation with the HT forcing averaged over SON. Individual dots correspond to each of the 10 ensemble members in the corresponding year and zonal wind (ZW) anomalies at 60°N averaged over DJF.

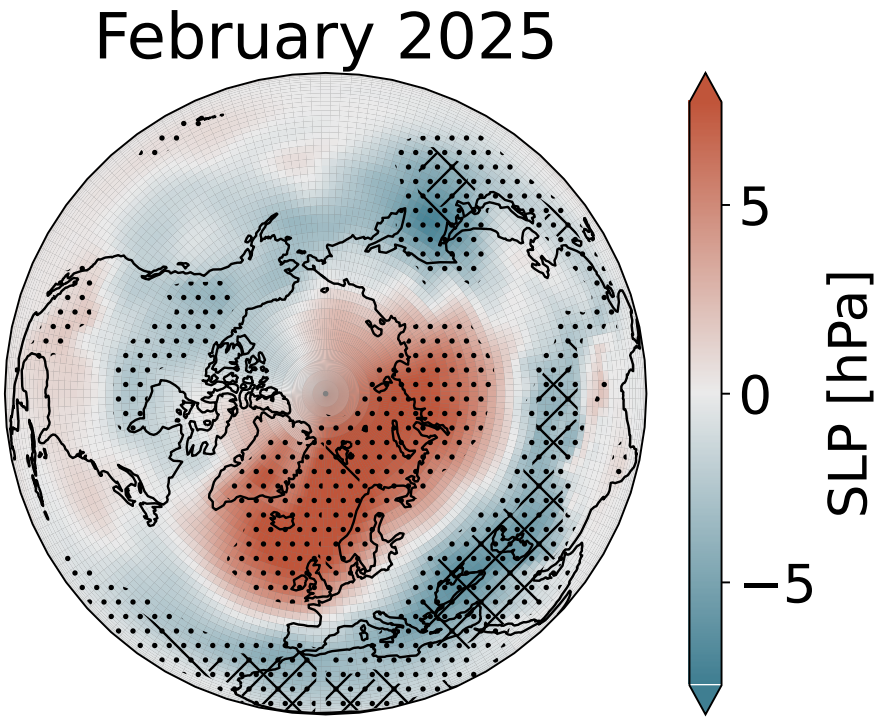


Figure 13. Monthly anomaly of sea level pressure (SLP in hPa) in February 2025 (MW3). Anomalies are expressed as the difference between the SOCOLv4 simulation with and without the HT forcing. Dots ... and hatching \\\\ and //// show where the p-values of the t-test are < 0.3 and < 0.1 and < 0.05, respectively.

5 Discussion and summary

Our study addresses the question of whether the anomalously strong Northern Hemisphere stratospheric polar vortex ~~(SPV)~~ of the boreal winter 2024/2025 has been linked to lingering dynamical and radiative impacts of the HT eruption. For this time period, satellite data show a coherent descent of HT-related water-vapour anomalies into the high-latitude stratosphere, collocated with a marked reduction in ozone and pronounced cold anomalies in the upper stratosphere and lower mesosphere. We detail that an ensemble of SOCOLv4 simulations, with the HT forcing, is able to reproduce the main spatial patterns of this WV plume and associated ozone response. Furthermore, through offline radiative transfer calculations, we show that the WV and ozone anomalies are, in combination, sufficient to generate substantial radiative cooling, which sharpens the meridional temperature gradient (see Fig. 14) and strengthens polar stratospheric westerly winds through thermal-wind balance.

The proposed mechanism, in which excess WV from HT and associated ozone changes ~~drives~~ drive radiative cooling that preconditions the polar vortex, is partly analogous to the well-documented Southern Hemisphere response to Antarctic ozone depletion in the lower stratosphere (Haase et al., 2020) and effects driven by energetic particle precipitation from mesospheric levels downward (Seppälä et al., 2025). Here, however, excess stratospheric WV from HT is considered as a joint driver

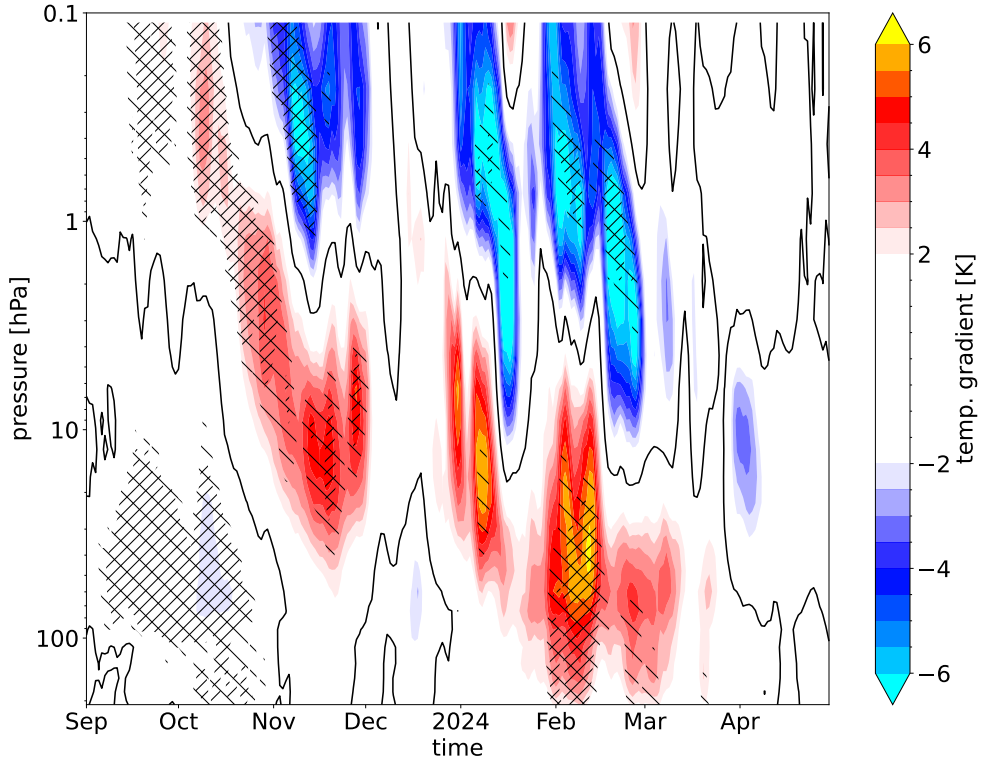


Figure 14. As Fig. 5, but daily anomalies of the weighted meridional temperature gradient (K) between lower (0–20°N) and polar (60–90°N) latitude bands for the extended winter 2023/2024 (MW2) from SOCOLv4. Anomalies are calculated as the difference between the SOCOLv4 simulation with and without the HT forcing. Hatching \\\\ and //// indicates where the p-values of the t-test are < 0.1 and < 0.05, respectively. Black contour line represents the zero anomaly.

together with slow Brewer–Dobson descent of the HT WV anomaly, enhanced HO_x and ClO_x chemistry leading to upper-stratospheric/mesospheric ozone loss, and the resulting longwave and shortwave cooling where WV and ozone anomalies overlap. This cooling ~~steepens the high-latitude~~ at the high latitudes steepens the meridional temperature gradient and, via the thermal-wind balance, favours a strong-vortex regime. At the same time, the response is strongly nonlinear: early-autumn wave activity can still transiently weaken the vortex, but once the radiatively strengthened westerlies have reached critical strength, additional wave forcing shows limited impact.

Taken together, the observations and paired SOCOLv4 simulations support a ~~forced tendency rather than deterministic attribution~~probabilistic interpretation: HT-related WV and ozone anomalies increased the likelihood of a stronger polar vortex while internal variability remains too large to attribute the full evolution of the observed and simulated winters to the HT forcing. Negative ozone and temperature anomalies can also arise dynamically in other strong-vortex winters; the distinctive feature of OW3 is the statistically significant HT-related WV tongue, partly overlapping with these anomalies. The weaker

and more variability-dominated MW3 response further indicates that both composition forcing and dynamical preconditioning matter.

Several limitations temper the interpretation and generality of these findings. ~~One reason is that the too fast~~ For one thing, the too-fast transport in SOCOLv4 causes the model to simulate the analogous 2024/2025 winter approximately one year earlier. SOCOLv4 also underestimates the amplitude of the HT-induced WV anomaly when compared with satellite records, implying that our simulated radiative cooling and dynamical response are likely conservative. However, SOCOLv4 agrees well with other models (Zhuo et al., 2025) in terms of the water vapor e-folding time (cf. Kuchar et al., 2025, Section A1). ~~The~~ Further, the radiative cooling and heating estimates rely on idealized offline calculations and thus cannot fully capture the coupling between radiation, atmospheric composition, and dynamics. ~~Our~~ In addition, our analysis is also based on a single model with a specific configuration (Sukhodolov et al., 2021, and references therein). ~~In addition~~Also, internal variability associated with ENSO and other tropospheric sources of internal variability may be only partially sampled by 10 ensemble members (e.g. Bittner et al., 2016a; Bednarz et al., 2026). On the other hand, a sufficiently strong (volcanic) forcing can produce a robust, stronger-than-average NH polar vortex (Bittner et al., 2016b).

Despite these caveats, our findings support the view that HT-induced WV and ozone anomalies have become an important multi-year driver of high-latitude winter variability. In fact, our current study and previous research detail a clear dichotomy: manifesting on the early-time scale as SPV weakening (Kuchar et al., 2025) and on the long-time scale as SPV strengthening. Furthermore, ~~looking ahead,~~ our ensemble simulations ~~suggest~~ indicated that as the WV plume continues to descend and QBO/ENSO conditions evolve, the balance between strong-vortex winters and SSW-prone winters ~~may shift~~ shifted once more in 2025/2026 because of the ~~upcoming~~ weaker WV forcing (see recent observed WV (less than 1 ppmv), ozone and temperature anomalies in Fig. 15), with corresponding impacts on surface patterns. More generally, unprecedented eruptions like HT may act as intermittent “sources of predictability” also called "windows of forecast opportunity" for polar winter circulation (Rupp et al., 2025, and references therein), albeit in a fundamentally probabilistic sense.

Future work should therefore (i) extend the analysis to coordinated multi-model HT experiments as in APARC (2025), (ii) investigate how volcanic moistening interacts with ongoing anthropogenic climate change to shape the statistics of SPV strength and SSW occurrence over the coming decades. Better constraining the structure and transport of the descending WV plume using MLS on NASA’s Aura satellite may be problematic due to the "duty cycle" of the 190-GHz observations to conserve remaining life for these measurements. Its decommissioning will cause a substantial gap in the measurement of critical atmospheric components such as WV and poses significant challenges for continuous monitoring and assessment of the effects of future extreme events including volcanic eruptions (Salawitch et al., 2025). However, other satellite (Knowland et al., 2025; Himes et al., and ground-based (De Mazière et al., 2018) instruments can continue to monitor WV after Aura MLS, respectively.

Code and data availability. SWOOSHv2.7 data can be downloaded from https://csl.noaa.gov/groups/csl8/swoosh/. The MERRA2 reanalysis dataset postprocessed by the NASA Ozone Watch can be downloaded for zonal wind and eddy heat flux from https://ozonewatch.gsfc.nasa.gov/meteorology/figures/merra2/wind/u60n_10_2024_merra2.txt and https://ozonewatch.gsfc.nasa.gov/meteorology/figures/merra2/heat_flux/

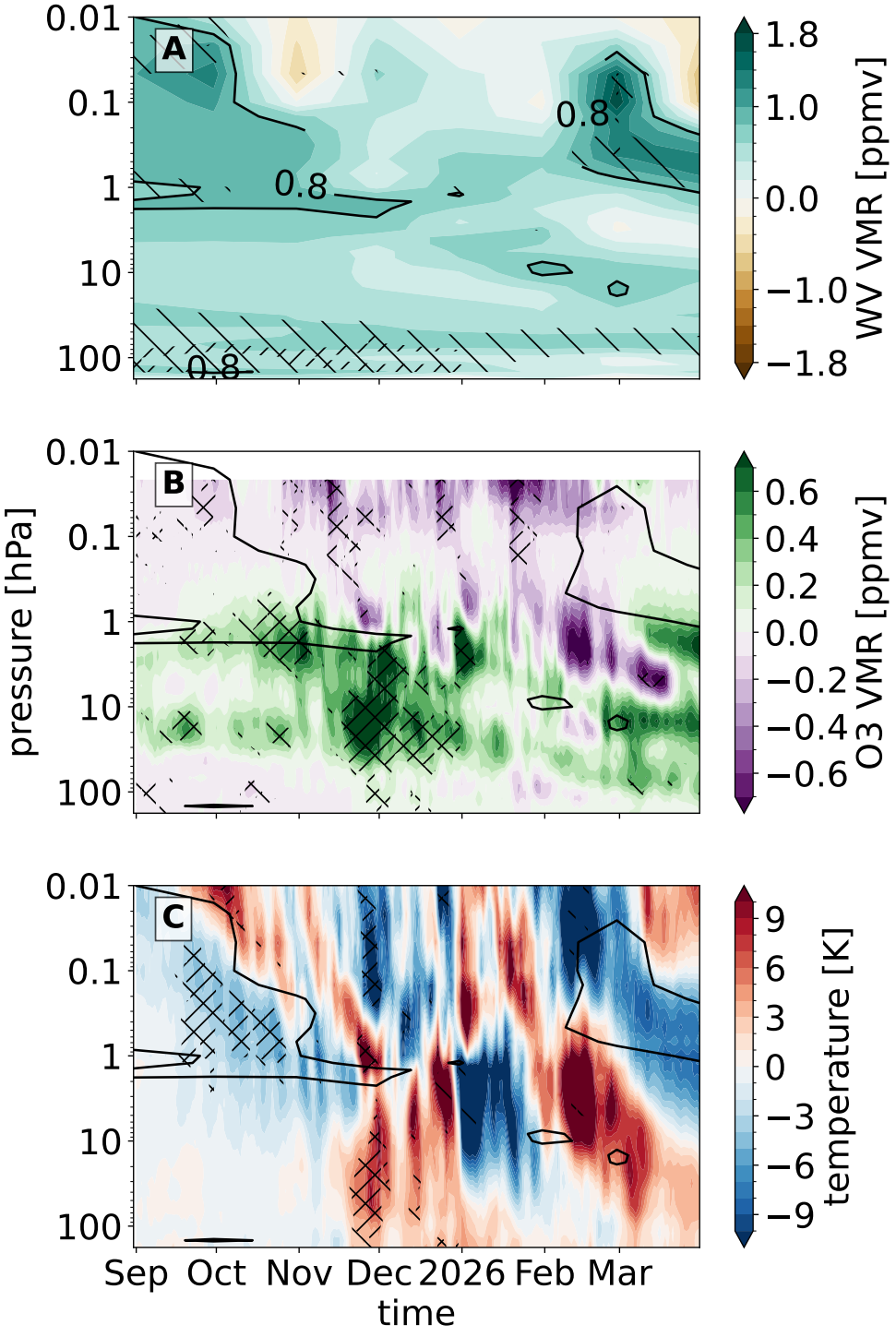


Figure 15. As Fig. 3 but for the extended winter 2025/2026 (OW4).

vt45_75-45n_100_2024_merra2.txt, respectively. Any direct access to full simulation data can be arranged by contacting the authors. The code that was used to produce all plots in this study is available via Zenodo (Kuchar et al., 2026). All postprocessed data files for this study are provided via Mendeley Data (Kuchar, 2026).

6 ~~Methods~~

~~Globally averaged water vapour (WV) anomalies (shading and brown contours for 0.5 and 1 ppmv) in SOCOLv4, MLSv6 and SWOOSH for the period 202201–202511. The 10–8 hPa artifact (Millán et al., 2024) in WV is still apparent in SWOOSH since it contains data from MLSv5. 0 (Davis et al., 2016a).~~

~~Monthly zonal-mean anomalies of polar chemistry for the period 2023/2024 (MW2). Anomalies are expressed as the difference between the SOCOLv4 simulation with and without the HT forcing. Hatching \\\\ and //// show where the p-values of the t-test are < 0.1 and < 0.05, respectively.~~

~~As Fig. 3 but for the extended winter 2025/2026 (OW4).~~

~~As Fig. 3 but for the extended winter 2023/2024 (OW2).~~

5.1 ~~Observational datasets~~

5.0.1 ~~MERRA2~~

~~We visualized meteorological variables (zonal wind and eddy heat flux) from the MERRA2 reanalysis (Gelaro et al., 2017) postprocessed by the NASA Ozone Watch (Kramarova and Lait, 2025) for the winter 2024/2025 (see Fig. 1).~~

5.0.1 ~~MLS~~

~~The Microwave Limb Sounder (MLS; Waters et al., 2006) instrument onboard NASA's Aura satellite has been operational since 2004 and provides near global (82°S—82°N) measurements of key atmospheric constituents and temperature based on thermal microwave emissions along the Earth's limb. The MLS provides about 3500 vertical profiles per day for each species. The profiles have a vertical resolution of approximately 3 to 5 km in the stratosphere and 6 to 8 km in the mesosphere. In this study, we use Version 6 of the retrieval products for water vapor, ozone, and temperature (Livesey et al., 2026).~~

~~Since May 2024, the 190 GHz subsystem in MLS, which is responsible for observing water vapor, N_2O, HCN, and upper stratospheric HNO_3, has been operating on a duty cycle to extend the instrument's lifetime (see). The measurements are reactivated for about six days in the middle of each calendar month. Other MLS channels, including those used for ozone and temperature, remain unaffected.~~

~~Water vapor, temperature and ozone data are processed using the recommended MLS quality screening (QS) criteria.~~

5.0.1 ~~SWOOSH~~

The Stratospheric Water and Ozone Satellite Homogenized (SWOOSH) version 2.72 dataset provides zonally averaged monthly profiles for water vapor and ozone. SWOOSH combines measurements from several satellite sensors, including the Stratospheric Aerosol and Gas Experiment (SAGE II & III), the Upper Atmosphere Research Satellite Halogen Occultation Experiment (UARS HALOE), UARS MLS, and Aura MLS version 5.0. The retrieval artifact in the 10—8 hPa layer apparent in SWOOSH (see Fig. 2 and Niemeier et al. (2023); Millán et al. (2024)) has been corrected in the MLS data version 6 we use in this study. To account for measurement offsets and biases, the data records were homogenized using „reference" satellites during times in which observations of different satellite systems overlapped. The satellite that showed the best agreement with balloon-based measurements was chosen as a reference (Davis et al., 2016b).

5.1 SOCOLv4 simulations

Our set of SOCOLv4 (Sukhodolov et al., 2021) simulations comprises an ensemble of transient simulations with and without the HT forcing, with 5-year spin-up before the HT eruption. Both ensembles comprise 10 ensemble members. We stress that QBO is nudged in both simulations with and without the HT forcing (see Fig. 12). We can demonstrate a link between the equatorial ZW at 10 hPa (QBO phase) and the polar vortex in SOCOLv4, i.e. so called Holton-Tan mechanism (Holton and Tan, 1980). For a detailed description of our SOCOLv4 simulations, we refer to Section A1 in Kuchar et al. (2025).

As indicated in Kuchar et al. (2025), the anomalous WV following HT dissipates in SOCOLv4 more quickly, as seen in the observations (cf. globally averaged WV anomaly in SOCOLv4, MLSv6 and SWOOSH in Fig. 2) or the other models (Randel et al., 2024b). Note that the contour for 0.5 ppmv does not reach the year 2024 in SOCOLv4 as in SWOOSH. It is questionable whether this bias is due to a different initialization (Zhu et al., 2025) or a model bias related to the overly fast transport already reported in Sukhodolov et al. (2021); Arsenovic et al. (2019). This longstanding issue persists even in the newest generation of chemistry-climate models, and SOCOLv4 is consistent with other models across generations (Abalos et al., 2026). In overall, SOCOLv4 is adequate for broad NOx/HOx/ClOx -driven ozone depletion/recovery studies (Sukhodolov et al., 2021). The main remaining weaknesses are transport and mixing, photolysis at large solar zenith angles over the high latitudes southern hemisphere (e.g. Imanova et al., 2025).

5.1 Offline radiative transfer simulations

We prescribed WV and ozone anomalies from MLS for the extended winter 2024/2025 (OW3) and calculated longwave and shortwave radiative heating rates using *konrad* (Kluft et al., 2019; Dacie et al., 2019). See all outputs in Fig. 9. *Konrad* uses interfaces the Rapid Radiative Transfer (RT) Model for GCMs (RRTMG Kroll et al., 2021). We state that these radiative calculations are robust for various solar zenith angles.

RRTMG radiative heating rates (longwave, shortwave and their sum) for prescribed weighted zonally-average over 60°–90°N of water vapour and ozone monnthyl anomalies from MLS for the extended winter 2024/2025 (OW3).

The RT calculations are fed with observed WV and O_3 anomaly profiles from MLS. Doing so, we yield negative anomalies in longwave heating rates (of less than $-0.5\,\mathrm{K/day}$) throughout the atmospheric layers. These anomalies correspond to the

prescribed positive WV anomalies. The RT calculations also yield negative anomalies for shortwave heating rates (exceeding $-1\,\mathrm{K/day}$) in the lower mesosphere. These anomalies emerge as a consequence of the prescribed negative ozone anomalies.

We confirm these calculations using precise line-by-line RT simulations (Bell et al., 2025). The resulting longwave heating rates from prescribed time-evolving WV and ozone from SOCOLv4 are shown in Fig. 10.

Weighted zonally-average over 60°–90°N of clear-sky (offline) longwave heating rate (in $\mathrm{K\,day^{-1}}$) anomalies calculated using solely WV (shading in **A**); WV and O_3 (shading in **B**). Contour in all panels represents a WV anomaly (0.5 ppmv) as in Figure 5. Anomalies are expressed as the difference between the SOCOLv4 simulation with and without the HT forcing. Hatching \\\\ and //// show where the p-values of the t-test are < 0.1 and < 0.05, respectively.

As detailed in Bloxam and Huang (2021), the radiative-cooling recovery of SSW-induced temperature anomalies in the absence of dynamical heating is dominated by longwave radiative cooling, and is characterized by increasing e-folding times from the upper to middle stratosphere. If we invert the e-folding times ($4 - 7.5\,\mathrm{days}$ in the upper stratosphere) of Bloxam and Huang (2021), we obtain an equivalent heating-rate effect of roughly $0.13 - 0.25\,\mathrm{K \cdot day^{-1}}$ per K. Given that the e-folding time increases in the lower stratosphere and decreases in the mesosphere, we expect that temperature perturbations translate into weaker and stronger heating-rate effects at lower and upper levels, respectively. In the lower stratosphere, the air cools more slowly because there is a deeper layer of atmosphere above it that absorbs the radiation, re-emits it upwards but also downwards, and thereby effectively reduces the amount of energy that can escape into space. Closer to the tropopause, the cooling effect reduces as the radiation emitted depends strongly on the background temperature itself (Bloxam and Huang, 2021). This asymmetry may explain the differing persistence in the heating rate anomalies at different heights Fig. 10**B**. Furthermore, the pronounced positive heating rate anomaly around 1 hPa spanning from December 2024 to March 2025, consistent with enhanced short wave absorption related to increased ozone, aids explaining the rapid change from negative to positive temperature anomalies (see Fig. 3**B** and Fig. 5**C**).

5.1 Calculation of anomalies

Throughout our analysis, we evaluate significance fields using the minimum local p-values from Student's t-test with global test statistics. All illustrations in Section 4 show differences between simulations with and without the HT forcing.

5.1 Eliassen-Palm flux diagnostics

The response of resolved waves is investigated using the Eliassen-Palm flux diagnostics (EPF; Andrews and McIntyre, 1987). EP fluxes are computed and scaled following Jucker (2021). The EPF convergence serves as an indicator of wave dissipation, and the EPF divergence (EPFD) indicates sourcing. We illustrate all EPF diagnostics from 2023-10-01 to 2024-03-30 in supplementary figure .

5.1 Calculation of Southern Oscillation Index (SOI)

We calculate the Southern Oscillation Index (SOI) using sea level pressure as a proxy for the El Niño Southern Oscillation. See particular years and corresponding SOI values in Fig. 12.

Scatter plot of equatorial zonal wind at 10 hPa as a proxy for Quasi-biennial Oscillation (QBO) in SOCOLv4 and Southern Oscillation Index (SOI) in the simulation with the HT forcing averaged over SON. Individual dots correspond to each of the 10 ensemble members in the corresponding year and zonal wind (ZW) anomalies at 60°N averaged over DJF.

5.1 QBO and ENSO preconditioning

The episode with the weakened ZW as a consequence of anomalously high EHF in December 2024 (MW3 in Fig. 6) and the beginning of January 2025 can be traced back to two main clusters of ensemble members in the simulations with the HT forcing (see Fig. 11). While one major cluster of 4 ensemble members (with mixed Southern Oscillation Index (SOI) preconditioning) strengthens SPV, the other cluster of 6 ensemble members (with mostly positive SOI (see Section 3.4 and Fig. 12) corresponding to La Niña preconditioning) weakens the stratospheric winds leading to the emergence of SSWs between December 2024 and January 2025. Considering the easterly phase of the Quasi-Biennial Oscillation (QBO) at 10 hPa for MW3, we hypothesize that this may have preconditioned the latter cluster to a higher probability of weaker SPV or SSWs, respectively. Such interpretation is consistent with the observation that SSWs are more likely to occur during easterly QBO in tandem with either El Niño or La Niña conditions (Lee et al., 2025).

That said, the simulated equatorial winds in the westerly QBO phase during the early stage of MW2 (see Fig. 12) create conditions that favor a stronger SPV, consistent with the Holton–Tan mechanism (Holton and Tan, 1980). A similar configuration occurred in OW3, when the QBO was also in its westerly phase[3]. Since the QBO preconditioning is identical in both simulations (with and without the HT forcing) and ENSO is uniformly sampled in SOCOLv4, encompassing both El Niño (SOI<0) and La Niña (SOI>0; as ultimately observed in OW3), we infer that the forced SPV response in MW2 arises from the HT-induced WV compared to OW3 where perhaps both QBO and the HT forcing contributed to the stronger SPV.

From the SOCOLv4 ensemble, yielding one cluster with easterly QBO and La Nina conditions in MW3, we hypothesize that the winter 2025/2026 (OW4) bears an enhanced probability of SSW occurrence. As the associated wind pattern propagates downward, we consequently identify a sea level pressure (SLP) pattern characteristic of a weaker SPV, i.e., a positive SLP anomaly at the poles and a negative SLP anomaly at the mid-latitudes (see Fig. 13).

Daily zonal-mean zonal wind at 10 hPa and 60°N based on the SOCOLv4 simulation with (ensemble mean (EM); red solid line) and without (black solid line) the HT forcing for the period 2024/2025 (MW3). The SOCOLv4 simulation with the HT forcing reveals two clusters: weak SPV (red dotted line) and strong SPV (red dashed line).

Monthly anomaly of sea level pressure (SLP in hPa) in February 2025 (MW3). Anomalies are expressed as the difference between the SOCOLv4 simulation with and without the HT forcing. Dots ... and hatching \\\\ and //// show where the p-values of the t-test are < 0.3 and < 0.1 and < 0.05, respectively.

Weighthed zonally-average over 60°–90°N of age of air estimated as idealized age tracer volume mixing ratio monthly anomalies for the extended winter 2023/2024 (MW2). Anomalies are expressed as the difference between the SOCOLv4

[3]

simulation with and without the HT forcing and normalized to its climatological standard deviation (SD). Dots ... and hatching \\\\ and //// show where the p-values of the t-test are < 0.3 and < 0.1 and < 0.05, respectively. The black contour line represents the contour of 1 ppmv of water vapour anomaly.

Author contributions. AK designed the study. TS set up and carried out the model simulations. AK analysed the data. AK, BL, JKH, TS, MS, and AB curated the data. AK compiled the manuscript with inputs from all other authors.

Competing interests. The authors declare that they have no conflict of interest.

Acknowledgements. ER has been supported by St. Petersburg State University under research grant 124032000025-1. MS was funded by the University of Graz, Graz, Austria. AB has been supported by the "Swiss H2O Hub for High-quality water vapor measurements from ground to space" project financed by GAW Switzerland. GC was funded by the European Union via the ERC Starting Grant (grant no. 101078127).

References

Abalos, M., Birner, T., Chrysanthou, A., Davis, S., de la Cámara, A., Dhomse, S., Garny, H., Hegglin, M. I., Hubert, D., Ivaniha, O., Keeble, J., Linz, M., Minganti, D., Neu, J., Plummer, D., Saunders, L., Shah, K., Stiller, G., Tourpali, K., Waugh, D., Abraham, N. L., Akiyoshi, H., Chipperfield, M. P., Jöckel, P., Josse, B., Morgenstern, O., Sukhodolov, T., Watanabe, S., and Yamashita, Y.: Evaluation of stratospheric transport in three generations of Chemistry-Climate Models, EGUsphere, 2026, 1–61, https://doi.org/10.5194/egusphere-2025-6549, 2026.

Andrews, D. G. and McIntyre, M. E.: JR Holton, and CB Leovy, 1987: Middle Atmosphere Dynamics, 1987.

APARC: The Hunga Volcanic Eruption Atmospheric Impacts Report, APARC Report 11, World Climate Research Programme (WCRP), https://doi.org/10.34734/FZJ-2025-05237, wCRP Report 10/2025, 2025.

Arsenovic, P., Damiani, A., Rozanov, E., Funke, B., Stenke, A., and Peter, T.: Reactive nitrogen (NO_y) and ozone responses to energetic electron precipitation during Southern Hemisphere winter, Atmospheric Chemistry and Physics, 19, 9485–9494, https://doi.org/10.5194/acp-19-9485-2019, 2019.

Bednarz, E. M., Butler, A. H., Wang, X., Zhuo, Z., Yu, W., Stenchikov, G., Toohey, M., and Zhu, Y.: Indirect climate impacts of the Hunga eruption, Atmospheric Chemistry and Physics, 26, 197–215, https://doi.org/10.5194/acp-26-197-2026, 2026.

Bell, A., Murk, A., and Stober, G.: Radiative impact of increased middle atmospheric water vapour in the aftermath of the Hunga 2022 volcanic eruption at two locations in the Northern Hemisphere, EGUsphere, 2025, 1–22, https://doi.org/10.5194/egusphere-2025-1396, 2025.

Bittner, M., Schmidt, H., Timmreck, C., and Sienz, F.: Using a large ensemble of simulations to assess the Northern Hemisphere stratospheric dynamical response to tropical volcanic eruptions and its uncertainty, Geophysical Research Letters, 43, 9324–9332, https://doi.org/https://doi.org/10.1002/2016GL070587, 2016a.

Bittner, M., Timmreck, C., Schmidt, H., Toohey, M., and Krüger, K.: The impact of wave-mean flow interaction on the Northern Hemisphere polar vortex after tropical volcanic eruptions, Journal of Geophysical Research: Atmospheres, 121, 5281–5297, https://doi.org/https://doi.org/10.1002/2015JD024603, 2016b.

Bloxam, K. and Huang, Y.: Radiative Relaxation Time Scales Quantified from Sudden Stratospheric Warmings, Journal of the Atmospheric Sciences, 78, 269 – 286, https://doi.org/10.1175/JAS-D-20-0015.1, 2021.

Brasseur, G. P. and Solomon, S.: Aeronomy of the middle atmosphere: Chemistry and physics of the stratosphere and mesosphere, vol. 32, Springer Science & Business Media, 2005.

Charney, J. G. and Drazin, P. G.: Propagation of planetary-scale disturbances from the lower into the upper atmosphere, Journal of Geophysical Research, 66, 83–109, 1961.

Clough, S. A. and Iacono, M. J.: Line-by-line calculation of atmospheric fluxes and cooling rates: 2. Application to carbon dioxide, ozone, methane, nitrous oxide and the halocarbons, Journal of Geophysical Research: Atmospheres, 100, 16 519–16 535, 1995.

Dacie, S., Kluft, L., Schmidt, H., Stevens, B., Buehler, S. A., Nowack, P. J., Dietmüller, S., Abraham, N. L., and Birner, T.: A 1D RCE Study of Factors Affecting the Tropical Tropopause Layer and Surface Climate, Journal of Climate, 32, 6769 – 6782, https://doi.org/10.1175/JCLI-D-18-0778.1, 2019.

Davis, S. M., Rosenlof, K. H., Hassler, B., Hurst, D. F., Read, W. G., Vömel, H., Selkirk, H., Fujiwara, M., and Damadeo, R.: The Stratospheric Water and Ozone Satellite Homogenized (SWOOSH) database: a long-term database for climate studies, Earth System Science Data, 8, 461–490, https://doi.org/10.5194/essd-8-461-2016, 2016a.

Davis, S. M., Rosenlof, K. H., Hassler, B., Hurst, D. F., Read, W. G., Vömel, H., Selkirk, H., Fujiwara, M., and Damadeo, R.: The Stratospheric Water and Ozone Satellite Homogenized (SWOOSH) database: a long-term database for climate studies, Earth System Science Data, 8, 461–490, https://doi.org/10.5194/essd-8-461-2016, 2016b.

De Mazière, M., Thompson, A. M., Kurylo, M. J., Wild, J. D., Bernhard, G., Blumenstock, T., Braathen, G. O., Hannigan, J. W., Lambert, J.-C., Leblanc, T., McGee, T. J., Nedoluha, G., Petropavlovskikh, I., Seckmeyer, G., Simon, P. C., Steinbrecht, W., and Strahan, S. E.: The Network for the Detection of Atmospheric Composition Change (NDACC): history, status and perspectives, Atmospheric Chemistry and Physics, 18, 4935–4964, https://doi.org/10.5194/acp-18-4935-2018, 2018.

Evan, S., Brioude, J., Rosenlof, K. H., Gao, R.-S., Portmann, R. W., Zhu, Y., Volkamer, R., Lee, C. F., Metzger, J.-M., Lamy, K., Walter, P., Alvarez, S. L., Flynn, J. H., Asher, E., Todt, M., Davis, S. M., Thornberry, T., Vömel, H., Wienhold, F. G., Stauffer, R. M., Millán, L., Santee, M. L., Froidevaux, L., and Read, W. G.: Rapid ozone depletion after humidification of the stratosphere by the Hunga Tonga Eruption, Science, 382, eadg2551, https://doi.org/10.1126/science.adg2551, 2023.

Fleming, E. L., Newman, P. A., Liang, Q., and Oman, L. D.: Stratospheric Temperature and Ozone Impacts of the Hunga Tonga-Hunga Ha'apai Water Vapor Injection, Journal of Geophysical Research: Atmospheres, 129, e2023JD039 298, https://doi.org/https://doi.org/10.1029/2023JD039298, e2023JD039298 2023JD039298, 2024.

Funke, B., López-Puertas, M., Stiller, G. P., and von Clarmann, T.: Mesospheric and stratospheric NOy produced by energetic particle precipitation during 2002–2012, Journal of Geophysical Research: Atmospheres, 119, 4429–4446, https://doi.org/https://doi.org/10.1002/2013JD021404, 2014.

Gelaro, R., McCarty, W., Suárez, M. J., Todling, R., Molod, A., Takacs, L., Randles, C. A., Darmenov, A., Bosilovich, M. G., Reichle, R., Wargan, K., Coy, L., Cullather, R., Draper, C., Akella, S., Buchard, V., Conaty, A., da Silva, A. M., Gu, W., Kim, G.-K., Koster, R., Lucchesi, R., Merkova, D., Nielsen, J. E., Partyka, G., Pawson, S., Putman, W., Rienecker, M., Schubert, S. D., Sienkiewicz, M., and Zhao, B.: The Modern-Era Retrospective Analysis for Research and Applications, Version 2 (MERRA-2), Journal of Climate, 30, 5419 – 5454, https://doi.org/10.1175/JCLI-D-16-0758.1, 2017.

Haase, S., Fricke, J., Kruschke, T., Wahl, S., and Matthes, K.: Sensitivity of the Southern Hemisphere circumpolar jet response to Antarctic ozone depletion: prescribed versus interactive chemistry, Atmospheric Chemistry and Physics, 20, 14 043–14 061, https://doi.org/10.5194/acp-20-14043-2020, 2020.

Himes, M. D., Kramarova, N. A., Wargan, K., Davis, S. M., and Jaross, G.: Continuing the MLS water vapor record with OMPS LP, EGUsphere, 2025, 1–24, https://doi.org/10.5194/egusphere-2025-4845, 2025.

Holton, J. R. and Tan, H.-C.: The influence of the equatorial quasi-biennial oscillation on the global circulation at 50 mb, Journal of Atmospheric Sciences, 37, 2200–2208, 1980.

Imanova, A., Egorova, T., Zubov, V., Mironov, A., Polyakov, A., Nerobelov, G., and Rozanov, E.: Seasonal Cycle of the Total Ozone Content over Southern High Latitudes in the CCM SOCOLv3, Atmosphere, 16, https://doi.org/10.3390/atmos16101172, 2025.

Jenkins, S., Smith, C., Allen, M., and Grainger, R.: Tonga eruption increases chance of temporary surface temperature anomaly above 1.5° C, Nature Climate Change, 13, 127–129, 2023.

Joshi, M. M., Charlton, A. J., and Scaife, A. A.: On the influence of stratospheric water vapor changes on the tropospheric circulation, Geophysical Research Letters, 33, https://doi.org/https://doi.org/10.1029/2006GL025983, 2006.

Jucker, M.: Scaling of Eliassen-Palm flux vectors, Atmospheric Science Letters, 22, e1020, https://doi.org/https://doi.org/10.1002/asl.1020, 2021.

Keeble, J., Braesicke, P., Abraham, N. L., Roscoe, H. K., and Pyle, J. A.: The impact of polar stratospheric ozone loss on Southern Hemisphere stratospheric circulation and climate, Atmospheric Chemistry and Physics, 14, 13 705–13 717, https://doi.org/10.5194/acp-14-13705-2014, publisher: Copernicus GmbH, 2014.

Kluft, L., Dacie, S., Buehler, S. A., Schmidt, H., and Stevens, B.: Re-Examining the First Climate Models: Climate Sensitivity of a Modern Radiative–Convective Equilibrium Model, Journal of Climate, 32, 8111 – 8125, https://doi.org/10.1175/JCLI-D-18-0774.1, 2019.

Knowland, K. E., Wales, P. A., Wargan, K., Weir, B., Pawson, S., Damadeo, R., and Flittner, D.: Stratospheric Water Vapor Beyond NASA's Aura MLS: Assimilating SAGE III/ISS Profiles for a Continued Climate Record, Geophysical Research Letters, 52, e2024GL112 610, https://doi.org/https://doi.org/10.1029/2024GL112610, e2024GL112610 2024GL112610, 2025.

Kramarova, N. and Lait, L. R.: NASA Ozone Watch: 2025 Antarctic MERRA-2 Wind, https://ozonewatch.gsfc.nasa.gov/meteorology/ozone_2024_MERRA2_NH.html, last updated 2025-12-19 21:55:40Z, 2025.

Kroll, C. A. and Schmidt, A.: Indirect stratospheric moisture increase after a Pinatubo-magnitude eruption can be comparable to direct increase after 2022 Hunga, Communications Earth & Environment, 5, 497, 2024.

Kroll, C. A., Dacie, S., Azoulay, A., Schmidt, H., and Timmreck, C.: The impact of volcanic eruptions of different magnitude on stratospheric water vapor in the tropics, Atmospheric Chemistry and Physics, 21, 6565–6591, https://doi.org/10.5194/acp-21-6565-2021, 2021.

Kuchar, A.: Accompanying data to "Modulation of the Northern polar vortex by the Hunga Tonga-Hunga Ha'apai eruption and associated surface response" and "Was the strengthening of the Northern polar vortex in 2024/2025 associated with the Hunga Tonga eruption?", Mendeley Data, https://doi.org/10.17632/hb3whw3nfr.2, 2026.

Kuchar, A., Sukhodolov, T., Chiodo, G., Jörimann, A., Kult-Herdin, J., Rozanov, E., and Rieder, H. H.: Modulation of the northern polar vortex by the Hunga Tonga–Hunga Ha'apai eruption and the associated surface response, Atmospheric Chemistry and Physics, 25, 3623–3634, https://doi.org/10.5194/acp-25-3623-2025, 2025.

Kuchar, A., Lehner, B., and Kult-Herdin, J.: boku-met/HTHH_strengthening: First release of our code repository related to HT-induced SPV strengthening, https://doi.org/10.5281/zenodo.21514652, 2026.

Lawrence, Z. D., Perlwitz, J., Butler, A. H., Manney, G. L., Newman, P. A., Lee, S. H., and Nash, E. R.: The Remarkably Strong Arctic Stratospheric Polar Vortex of Winter 2020: Links to Record-Breaking Arctic Oscillation and Ozone Loss, Journal of Geophysical Research: Atmospheres, 125, e2020JD033 271, https://doi.org/https://doi.org/10.1029/2020JD033271, e2020JD033271 10.1029/2020JD033271, 2020.

Lee, S. H., Butler, A. H., and Manney, G. L.: Two major sudden stratospheric warmings during winter 2023/2024, Weather, 80, 45–53, https://doi.org/https://doi.org/10.1002/wea.7656, 2025.

Livesey, N., Read, W., Wagner, P., Santee, M., Froidevaux, L., Schwartz, M., Lambert, A., Millan, L., Werner, F., Pumphrey, H., Manney, G., Fuller, R., Jarnot, R., Knosp, B., and Vuu, B. C.: Earth Observing System (EOS) Aura Microwave Limb Sounder (MLS) Version 6.0x Level-2 and Level-3 data quality and description document, https://doi.org/10.5067/AURA/MLS/DOC/v6_dataqualitydocument, 2026.

Manney, G. L., Santee, M. L., Rex, M., Livesey, N. J., Pitts, M. C., Veefkind, P., Nash, E. R., Wohltmann, I., Lehmann, R., Froidevaux, L., et al.: Unprecedented Arctic ozone loss in 2011, Nature, 478, 469–475, https://doi.org/https://doi.org/10.1038/nature10556, 2011.

Manzini, E., Steil, B., Brühl, C., Giorgetta, M. A., and Krüger, K.: A new interactive chemistry-climate model: 2. Sensitivity of the middle atmosphere to ozone depletion and increase in greenhouse gases and implications for recent stratospheric cooling, Journal of Geophysical Research: Atmospheres, 108, https://doi.org/10.1029/2002JD002977, _eprint: https://agupubs.onlinelibrary.wiley.com/doi/pdf/10.1029/2002JD002977, 2003.

Matthias, V., Dörnbrack, A., and Stober, G.: The extraordinarily strong and cold polar vortex in the early northern winter 2015/2016, Geophysical Research Letters, 43, 12,287–12,294, https://doi.org/https://doi.org/10.1002/2016GL071676, 2016.

Maycock, A. C., Joshi, M. M., Shine, K. P., and Scaife, A. A.: The Circulation Response to Idealized Changes in Stratospheric Water Vapor, Journal of Climate, 26, 545 – 561, https://doi.org/10.1175/JCLI-D-12-00155.1, 2013.

Millán, L., Santee, M. L., Lambert, A., Livesey, N. J., Werner, F., Schwartz, M. J., Pumphrey, H. C., Manney, G. L., Wang, Y., Su, H., Wu, L., Read, W. G., and Froidevaux, L.: The Hunga Tonga-Hunga Ha'apai Hydration of the Stratosphere, Geophysical Research Letters, 49, e2022GL099 381, https://doi.org/https://doi.org/10.1029/2022GL099381, e2022GL099381 2022GL099381, 2022.

Millán, L., Read, W. G., Santee, M. L., Lambert, A., Manney, G. L., Neu, J. L., Pitts, M. C., Werner, F., Livesey, N. J., and Schwartz, M. J.: The Evolution of the Hunga Hydration in a Moistening Stratosphere, Geophysical Research Letters, 51, e2024GL110 841, https://doi.org/https://doi.org/10.1029/2024GL110841, e2024GL110841 2024GL110841, 2024.

Newman, P. A., Nash, E. R., and Rosenfield, J. E.: What controls the temperature of the Arctic stratosphere during the spring?, Journal of Geophysical Research: Atmospheres, 106, 19 999–20 010, https://doi.org/https://doi.org/10.1029/2000JD000061, 2001.

Niemeier, U., Wallis, S., Timmreck, C., van Pham, T., and von Savigny, C.: How the Hunga Tonga—Hunga Ha'apai Water Vapor Cloud Impacts Its Transport Through the Stratosphere: Dynamical and Radiative Effects, Geophysical Research Letters, 50, e2023GL106 482, https://doi.org/https://doi.org/10.1029/2023GL106482, e2023GL106482 2023GL106482, 2023.

Plumb, R. A.: On the seasonal cycle of stratospheric planetary waves, Pure and applied geophysics, 130, 233–242, 1989.

Proud, S. R., Prata, A. T., and Schmauß, S.: The January 2022 eruption of Hunga Tonga-Hunga Ha'apai volcano reached the mesosphere, Science, 378, 554–557, https://doi.org/10.1126/science.abo4076, 2022.

Randel, W. J., Podglajen, A., and Wu, F.: Stratospheric Transit Time Distributions Derived From Satellite Water Vapor Measurements, Journal of Geophysical Research: Atmospheres, 129, e2024JD041 595, https://doi.org/https://doi.org/10.1029/2024JD041595, e2024JD041595 2024JD041595, 2024a.

Randel, W. J., Wang, X., Starr, J., Garcia, R. R., and Kinnison, D.: Long-Term Temperature Impacts of the Hunga Volcanic Eruption in the Stratosphere and Above, Geophysical Research Letters, 51, e2024GL111 500, https://doi.org/10.1029/2024GL111500, _eprint: https://onlinelibrary.wiley.com/doi/pdf/10.1029/2024GL111500, 2024b.

Rieder, H., Kult-Herdin, J., Polvani, L. M., Solomon, S., and Kuchar, A.: Are springtime Arctic ozone columns predictable from wintertime conditions?, Frontiers in Earth Science, 13, 1610 651, https://doi.org/https://doi.org/10.3389/feart.2025.1610651, 2025.

Rupp, P., Spaeth, J., and Birner, T.: A spread-versus-error framework to reliably quantify the potential for subseasonal windows of forecast opportunity, EGUsphere, 2025, 1–24, https://doi.org/10.5194/egusphere-2025-4925, 2025.

Salawitch, R. J., Smith, J. B., Selkirk, H., Wargan, K., Chipperfield, M. P., Hossaini, R., Levelt, P. F., Livesey, N. J., McBride, L. A., Millán, L. F., Moyer, E., Santee, M. L., Schoeberl, M. R., Solomon, S., Stone, K., and Worden, H. M.: The Imminent Data Desert: The Future of Stratospheric Monitoring in a Rapidly Changing World, Bulletin of the American Meteorological Society, 106, E540 – E563, https://doi.org/10.1175/BAMS-D-23-0281.1, 2025.

Schoeberl, M. R., Wang, Y., Ueyama, R., Dessler, A., Taha, G., and Yu, W.: The Estimated Climate Impact of the Hunga Tonga-Hunga Ha'apai Eruption Plume, Geophysical Research Letters, 50, e2023GL104 634, https://doi.org/10.1029/2023GL104634, 2023.

Schoeberl, M. R., Toohey, M., Wang, Y., and Ueyama, R.: Stratospheric Injection Lifetimes, Journal of Geophysical Research: Atmospheres, 130, e2025JD043 928, https://doi.org/https://doi.org/10.1029/2025JD043928, e2025JD043928 2025JD043928, 2025.

Scott, R. and Haynes, P.: The seasonal cycle of planetary waves in the winter stratosphere, Journal of the atmospheric sciences, 59, 803–822, 2002.

Seabrook, M., Smith, D. M., Dunstone, N. J., Eade, R., Hermanson, L., Scaife, A. A., and Hardiman, S. C.: Opposite Impacts of Interannual and Decadal Pacific Variability in the Extratropics, Geophysical Research Letters, 50, e2022GL101 226, https://doi.org/https://doi.org/10.1029/2022GL101226, e2022GL101226 2022GL101226, 2023.

Seppälä, A., Kalakoski, N., Verronen, P. T., Marsh, D. R., Karpechko, A. Y., and Szelag, M. E.: Polar mesospheric ozone loss initiates downward coupling of solar signal in the Northern Hemisphere, Nature Communications, 16, 748, 2025.

Stenchikov, G., Ukhov, A., and Osipov, S.: Modeling the Radiative Forcing and Atmospheric Temperature Perturbations Caused by the 2022 Hunga Volcano Explosion, Journal of Geophysical Research: Atmospheres, 130, e2024JD041 940, https://doi.org/10.1029/2024JD041940, 2025.

Stocker, M., Steiner, A. K., Ladstädter, F., Foelsche, U., and Randel, W. J.: Strong persistent cooling of the stratosphere after the Hunga eruption, Communications Earth & Environment, 5, 450, https://doi.org/https://doi.org/10.1038/s43247-024-01620-3, 2024.

Sukhodolov, T., Egorova, T., Stenke, A., Ball, W. T., Brodowsky, C., Chiodo, G., Feinberg, A., Friedel, M., Karagodin-Doyennel, A., Peter, T., Sedlacek, J., Vattioni, S., and Rozanov, E.: Atmosphere–ocean–aerosol–chemistry–climate model SOCOLv4.0: description and evaluation, Geoscientific Model Development, 14, 5525–5560, https://doi.org/10.5194/gmd-14-5525-2021, 2021.

Vömel, H., Evan, S., and Tully, M.: Water vapor injection into the stratosphere by Hunga Tonga-Hunga Ha'apai, Science, 377, 1444–1447, https://doi.org/10.1126/science.abq2299, 2022.

Waters, J. W., Froidevaux, L., Harwood, R. S., Jarnot, R. F., Pickett, H. M., Read, W. G., Siegel, P. H., Cofield, R. E., Filipiak, M. J., Flower, D. A., et al.: The earth observing system microwave limb sounder (EOS MLS) on the Aura satellite, IEEE transactions on geoscience and remote sensing, 44, 1075–1092, 2006.

Young, P. J., Butler, A. H., Calvo, N., Haimberger, L., Kushner, P. J., Marsh, D. R., Randel, W. J., and Rosenlof, K. H.: Agreement in late twentieth century Southern Hemisphere stratospheric temperature trends in observations and CCMVal-2, CMIP3, and CMIP5 models, Journal of Geophysical Research: Atmospheres, 118, 605–613, https://doi.org/10.1002/jgrd.50126, publisher: John Wiley & Sons, Ltd, 2013.

Zhou, X., Dhomse, S. S., Feng, W., Mann, G., Heddell, S., Pumphrey, H., Kerridge, B. J., Latter, B., Siddans, R., Ventress, L., Querel, R., Smale, P., Asher, E., Hall, E. G., Bekki, S., and Chipperfield, M. P.: Antarctic Vortex Dehydration in 2023 as a Substantial Removal Pathway for Hunga Tonga-Hunga Ha'apai Water Vapor, Geophysical Research Letters, 51, e2023GL107 630, https://doi.org/https://doi.org/10.1029/2023GL107630, e2023GL107630 2023GL107630, 2024.

Zhu, Y., Akiyoshi, H., Aquila, V., Asher, E., Bednarz, E. M., Bekki, S., Brühl, C., Butler, A. H., Case, P., Chabrillat, S., Chiodo, G., Clyne, M., Colarco, P. R., Dhomse, S., Falletti, L., Fleming, E., Johnson, B., Jörimann, A., Kovilakam, M., Koren, G., Kuchar, A., Lebas, N., Liang, Q., Liu, C.-C., Mann, G., Manyin, M., Marchand, M., Morgenstern, O., Newman, P., Oman, L. D., Østerstrøm, F. F., Peng, Y., Plummer, D., Quaglia, I., Randel, W., Rémy, S., Sekiya, T., Steenrod, S., Sukhodolov, T., Tilmes, S., Tsigaridis, K., Ueyama, R., Visioni, D., Wang, X., Watanabe, S., Yamashita, Y., Yu, P., Yu, W., Zhang, J., and Zhuo, Z.: Hunga Tonga–Hunga Ha'apai Volcano Impact Model Observation Comparison (HTHH-MOC) project: experiment protocol and model descriptions, Geoscientific Model Development, 18, 5487–5512, https://doi.org/10.5194/gmd-18-5487-2025, 2025.

Zhuo, Z., Wang, X., Zhu, Y., Yu, W., Bednarz, E. M., Fleming, E., Colarco, P. R., Watanabe, S., Plummer, D., Stenchikov, G., Randel, W., Bourassa, A., Aquila, V., Sekiya, T., Schoeberl, M. R., Tilmes, S., Zhang, J., Kushner, P. J., and Pausata, F. S. R.: Comparing multi-model ensemble simulations with observations and decadal projections of upper atmospheric variations following the Hunga eruption, Atmospheric Chemistry and Physics, 25, 13 161–13 176, https://doi.org/10.5194/acp-25-13161-2025, 2025.